J. Fluid Mech. (2011), *vol.* 680, *pp.* 114–149.
doi:10.1017/jfm.2011.153

Collective oscillations in bubble clouds

ZORANA ZERAVCIC[1]†, DETLEF LOHSE[2] AND WIM VAN SAARLOOS[1,3]

[1]Instituut Lorentz, University of Leiden, Niels Bohrweg 2, 2333 CA Leiden, The Netherlands

[2]Physics of Fluids Group, Mesa+ and Impact Research Institutes and Burgers Center for Fluid Dynamics, Department for Science and Technology, University of Twente, PO Box 217, 7500 AE Enschede, The Netherlands

[3]FOM Foundation, PO Box 3201, 3502 GA Utrecht, The Netherlands

(Received 21 June 2010; revised 14 March 2011; accepted 27 March 2011; first published online 6 June 2011)

In this paper the collective oscillations of a bubble cloud in an acoustic field are theoretically analysed with concepts and techniques of condensed matter physics. More specifically, we will calculate the eigenmodes and their excitabilities, eigenfrequencies, densities of states, responses, absorption and participation ratios to better understand the collective dynamics of coupled bubbles and address the question of possible localization of acoustic energy in the bubble cloud. The radial oscillations of the individual bubbles in the acoustic field are described by coupled linearized Rayleigh–Plesset equations. We explore the effects of viscous damping, distance between bubbles, polydispersity, geometric disorder, size of the bubbles and size of the cloud. For large enough clusters, the collective response is often very different from that of a typical mode, as the frequency response of each mode is sufficiently wide that many modes are excited when the cloud is driven by ultrasound. The reason is the strong effect of viscosity on the collective mode response, which is surprising, as viscous damping effects are small for single-bubble oscillations in water. Localization of acoustic energy is only found in the case of substantial bubble size polydispersity or geometric disorder. The lack of localization for a weak disorder is traced back to the long-range $1/r$ interaction potential between the individual bubbles. The results of the present paper are connected to recent experimental observations of collective bubble oscillations in a two-dimensional bubble cloud, where pronounced edge states and a pronounced low-frequency response had been observed, both consistent with the present theoretical findings. Finally, an outlook to future possible experiments is given.

Key words: bubble dynamics, waves in random media

1. Introduction

The dynamics of an isolated bubble in an acoustic field is well understood. It can theoretically be well described with the Rayleigh–Plesset equation and extensions thereof (Plesset & Prosperetti 1977; Prosperetti & Lezzi 1986; Leighton 1994; Brennen 1995). The experiments with a single stable sonoluminescing bubble have confirmed this theory (Brenner, Hilgenfeldt & Lohse 2002).

The situation is much more complicated for *interacting* bubbles. First, the sound emission of an oscillating bubble is felt by the neighbouring bubbles in a very large

† Email address for correspondence: zorana@seas.harvard.edu

range, as the corresponding Bjerknes potential only decays with $1/r$, where r is the distance between the bubbles (Leighton 1994; Brennen 1995). This bubble–bubble interaction leads to frequency shifts of the eigenfrequencies of the collective systems as compared to isolated bubbles (see e.g. Smereka & Banerjee 1988; d'Agostino & Brennen 1989; Brennen 2002; Ida 2005; Colonius *et al.* 2008 or the above-mentioned standard textbooks on bubbles), as is the case for any system of coupled oscillators (Landau & Lifshitz 1960). Second, oscillating bubbles attract or repel each other (depending on their mutual size and the driving pressure; Mettin *et al.* 1997; Doinikov & Zavtrak 1996; Ida 2004, 2005) thanks to the secondary Bjerknes forces (Leighton 1994; Brennen 1995). Interacting bubbles are however the genuine case in nature and technology (Leighton 1994, 2004), be it in underwater acoustics such as e.g. for underwater noise damping and absorption with the help of bubble clouds or curtains (Wursig, Greene & Jefferson 2000; Osborn *et al.* 1992), the (repelling) effect of bubble curtains on fish schools (Sharpe & Dill 1997), for the sound production of colonies of snapping shrimp (Versluis *et al.* 2000) and for submarine detection, or for sound propagation in bubbly liquids (van Wijngaarden 1972; Noordzij & van Wijngaarden 1974; Calflisch *et al.* 1985; Sangani & Didwania 1993; Wang & Brennen 1999; Smereka 2002; Colonius *et al.* 2008), for acoustic cavitation in bubble clouds (d'Agostino & Brennen 1988; Kumar & Brennen 1993; Parlitz *et al.* 1999), for ultrasound diagnostics with ultrasound contrast agents (Burns 1996; Mulvagh *et al.* 2000; Dayton *et al.* 2000; Qin & Ferrara 2006; van der Meer *et al.* 2007), for shock-wave lithotripsy (Arora, Junge & Ohl 2005; Arora, Ohl & Lohse 2007), for ultrasonic and megasonic cleaning (Busnaina, Kashkoush & Gale 1995; Krefting, Mettin & Lauterborn 2004; Zijlstra *et al.* 2009), or in the process industry. So further progress in the fundamental understanding of the collective behaviour of bubble clouds is desired.

Some progress could be achieved by eliminating the second of the above-mentioned complications, namely mutual bubble attraction or repulsion: by exposing air pockets in artificial crevices on a plain surface at well-defined distances to ultrasonic extension waves, Bremond *et al.* (2005, 2006*a, b*) studied the collective collapse of a bubble cloud with bubbles at fixed positions, thereby decoupling the radial oscillations from the translational dynamics of the coupled bubbles. They found that an extended Rayleigh–Plesset equation – with an extra term taking into consideration the sound emission of all other bubbles (Brennen 1995; Pelekasis *et al.* 2004; Doinikov 2004) – well describes the collective dynamics, provided that their mutual distance is large enough. Applying the same trick of trapping gas pockets in artificial crevices of geometrically patterned hydrophobic surfaces, but now driven with only small pressure amplitudes, Rathgen *et al.* (2007) studied collective modes of coupled oscillating micromenisci in a plane ('two-dimensional bubble cloud'), experimentally finding a resonance at much lower frequency as compared to the one of a single micromeniscus. The origin of the shift is due to the acoustic coupling of the oscillating micromenisci that produces collective modes.

The present work builds on the earlier papers (Bremond *et al.* 2006*a, b*; Rathgen *et al.* 2007) but aims at a more detailed and fundamental understanding of the spectrum and the response to driving. We will employ concepts and techniques of condensed matter physics which recently experienced a revival in soft condensed matter physics, successfully analysing vibrational modes in jammed systems (see e.g. Zeravcic, van Saarloos & Nelson 2008; Xu *et al.* 2009; Liu & Nagel 2010; van Hecke 2010; Vitelli *et al.* 2010). More specifically, the calculation of the eigenmodes and their excitabilities, eigenfrequencies, densities of states (DOS), responses, absorption and participation ratios turned out to be extremely useful to better understand the

dynamics of these jammed systems. We will show in this paper that this is also the case for the dynamics of coupled bubbles.

In particular, employing these concepts will allow us to address the possibility and the nature of *localization* of acoustic energy in bubble clouds. Localization has been identified in acoustic modes before (Sornette & Souillard 1988; Ye & Alvarez 1998) but never been analysed with the concepts and techniques of modern condensed matter physics. We want to compare the localization of energy in a bubble cloud with the classical Anderson localization (Anderson 1958) of waves in disordered condensed matter. Here localization refers to the fact that waves, which are extended (like plane waves) in the absence of disorder, can become localized in the presence of disorder. Then a localized state or eigenmode is concentrated around a point in space and has an amplitude that falls off exponentially with the distance from the centre. The occurrence of localized eigenmodes in systems that are described with wave-type equations is of a general nature and can be extended to many systems such as sound modes, gravity waves, diffusion on random lattices, etc. (Sheng 1995, 1990). It is therefore a natural question to ask whether localization also plays a major role in collective bubble oscillations, where the disorder can result both from the positional disorder of the bubble centres and from the bubble polydispersity. As we shall see, localization does play some role, but the effects are subtle, partly due to the long-range nature of the bubble–bubble interaction term, which is very different from the short-range interaction common in condensed matter physics. If the wave character of the pressure field is suppressed by ignoring the phase factor of the bubble–bubble interaction, we find power-law localization of the modes and response due to the power-law interaction. If, however, the phase factor is retained, we recover the exponential localization found by Sornette & Souillard (1988), Ye & Alvarez (1998) and Sornette & Legrend (1992), which is typical of systems with effectively short-range interactions.

The phase space to be explored is considerable, being spanned by bubble radius, polydispersity, viscosity, distance between the bubbles and the underlying structure of the bubble array. For simplicity and for better comparison with experiment, as in Bremond *et al.* (2006*b*), Bremond *et al.* (2006*a*) and Rathgen *et al.* (2007), we take the positions of the bubbles to be fixed. This however hardly limits the applicability of our approach and our results: whenever the period of the relevant resonance frequencies is much shorter than the time scale for rearrangements of the bubble cloud, an adiabatic approximation in which the positions of the bubbles are considered fixed suffices. This applies to many situations of practical interest.

Another simplification will be our restriction to the case of the *linearized* Rayleigh–Plesset equation, i.e. to weak driving $P_a \cos(\omega_d t)$, with a driving pressure amplitude P_a much smaller than the ambient pressure p_0^∞ (which normally is 1 bar) and ω_d the driving frequency. The main motivation is that resonance behaviour (which we want to explore) by definition is the behaviour of the linearized system and correspondingly our methods can only be applied to the linear case. As we will see, even in this linear case the phenomenology is rich (and complicated) enough. A full nonlinear treatment of the system is beyond the scope of the present paper.

In order to prepare the reader for the rich and large variety of effects which play a role and for the complexity of some of the mode behaviour, we already show in figure 1 a sample of the mode and response behaviour which can be found in coupled bubble oscillators at various frequencies. The details of this will be discussed later. The analysis of the full spectrum will reveal both the aforementioned low-energy collective modes with nearby bubbles oscillating in phase and modes with nearby

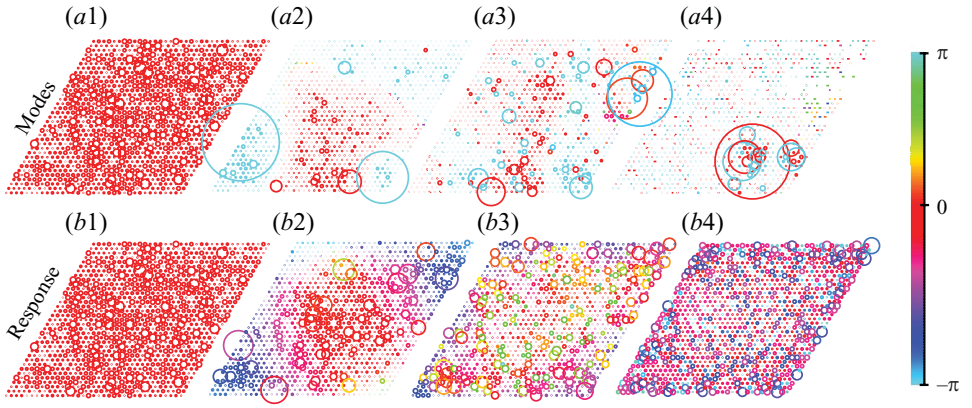

FIGURE 1. (Colour online available at journals.cambridge.org/FLM) Examples of eigenmodes and response fields for a system of $N = 1225$, 20 % polydisperse bubbles (with mean radius $R^0 = 5\,\mu\text{m}$), each of which is represented by a circle. The radii of the circles in the plot are proportional to the amplitude of the oscillation and the colour shows the phase. ($a1$–$a4$) Going from left to right: 1st, 7th, 107th and 807th modes, respectively. ($b1$–$b4$) Response of the system to uniform driving with the 1st, 7th, 107th and 807th eigenfrequencies, respectively.

bubbles oscillating in anti-phase that have resonant frequencies larger than those of individual bubbles. This contributes to the non-trivial DOS of the collective modes, which, as common in condensed matter physics, has profound consequences on the response. For better accessibility of the paper for the fluid dynamics community, we will explain the origin of these main features along figure 1 in an overview of the main ingredients of the dynamics of coupled bubble oscillations and response in § 2.

The paper is organized as follows: section 2 qualitatively discusses the various competing effects and summarizes and physically accounts for the main results. Section 3 is dedicated to the formalisms that we used to calculate the spectrum of a cluster of mono- and polydisperse bubbles, calculation of the response of these systems upon driving and definitions of the quantities we will use to address the properties of both the eigenvibrations and the response. Naturally, this section is rather technical. In § 4, we present the main results for the case of monodisperse clusters of bubbles positioned in regular ordered arrays. In § 5, we study the effect of the disorder introduced by polydispersity and briefly discuss the effects of making the underlying structure random. As the conclusions are already given in § 2, in the last section we restrict ourselves to an outlook on possible experiments to study collective behaviour of bubbles in bubbly clouds.

2. Qualitative discussion of the physical ingredients and competing effects and main results

The parameter space of coupled bubble oscillations is huge: bubble size and polydispersity, bubble distances, liquid viscosity, thermal diffusivity, surface tension and density, the corresponding material properties of the gas, and the geometry of bubble arrangements. Clearly, the parameter space is far too large to fully explore. So we must restrict ourselves to pinpoint the main trends and to isolate the most important effects. In order to guide the reader's intuition and to set the stage for the further analysis, in this section we will first summarize the most relevant parameters that affect the collective bubble oscillation problem and qualitatively summarize the main results.

2.1. *Single-bubble properties: resonance frequency, damping and Q-factor*

When surface tension effects are small (as is the case for bubbles larger than a few μm), the resonance frequency Ω^0 of a single bubble with ambient (i.e. static) radius R^0 is the Minnaert frequency (Brennen 1995)

$$\Omega^0 = \sqrt{3p_0^\infty/\rho}\,\frac{1}{R^0}, \tag{2.1}$$

where p_0^∞ is the ambient pressure and ρ is the density of the liquid. Its viscous damping rate Γ is given by

$$\Gamma = \frac{\mu}{\rho(R^0)^2}. \tag{2.2}$$

From the resonance frequency and the damping rate, one can define a quality $Q = \Omega^0/\Gamma$. For a bubble, one obtains

$$Q = \frac{\Omega^0}{\Gamma} = \frac{\sqrt{p_0^\infty \rho}}{\mu}\,R^0. \tag{2.3}$$

The Q-factor determines the sharpness of the resonance and response of an oscillator: the larger the Q, the more the response is peaked around its natural oscillation frequency Ω^0 (throughout this paper we will use the terms *sharpness of the resonance* and *Q-factor* interchangeably). An example of this behaviour is shown in figures 1(a1) and 1(b1): in (a1) we plot the lowest-frequency (collective) eigenmode, which is the least damped in the spectrum (see § 3.2 for details). Figure 1(b1) is a response of the system when uniformly driven with the lowest resonant frequency; the response field is hardly distinguishable from the single-mode behaviour in figure 1(a1). For the rest of the mode examples depicted in figure 1(a2–a4), the effect of damping is more pronounced, influencing the response, see figure 1(b2–b4). We come back to the origin of the different behaviour at low and high frequencies below.

For a given fluid, the Q-factor can be tuned by the bubble radius. For water at atmospheric pressure, the Q-factor is already about 5 for a bubble with a radius of only 1 μm. Hence single bubbles of sizes larger than a few μm are weakly damped, i.e. are sharp resonators: the effect of viscosity is small.

2.2. *Bubble–bubble interactions*

The coupling of bubble–bubble oscillations is mediated through the pressure field, which falls off inversely proportional to the distance from an oscillating bubble. This makes the interaction term very different from the short-ranged (near-neighbour-like) interactions that one usually encounters in condensed matter physics: here the interactions are long-ranged, and each bubble interacts with many others. This has several important consequences, one of which is that it appears to suppress the classical Anderson localization with exponentially decaying eigenmodes (see § 5.3 for details). An example of this behaviour is shown in figure 1(a4) where we depict a high-frequency eigenmode of a strongly disordered system (20 % polydispersity in the static bubble radii, see § 5.2): compared to high-frequency modes in other (standard) systems described by the wave equation, this mode does not only have a group of bubbles oscillating, but also a small-amplitude background coupled to it.

Other important implications are that the bubble–bubble interactions are never small in large clouds, as each bubble feels many others, and that the strength of the interactions, i.e. *interaction parameter* K, is essentially tuned by varying the ratio

$$K = \frac{\langle R^0 \rangle}{d}, \tag{2.4}$$

where $\langle R^0 \rangle$ is the average static bubble radius and d is the average distance between the bubbles (cf. Bremond *et al.* 2006*b*).

2.3. *The density of states*

The presence of interactions between the bubbles will lead to collective modes (like the ones in figure 1(*a*1)–1(*a*4)), which we can label with their resonance frequency. Like any damped harmonic oscillator, each mode will have a Lorentzian response curve whose width in frequency is of order $1/Q$. An important quantity for a large array of bubbles is the DOS, $D(\omega)$. For a cloud of N bubbles, $ND(\omega)\mathrm{d}\omega$ is the number of modes with resonance frequency between ω and $\omega + \mathrm{d}\omega$. In condensed matter theory, the DOS is quite important for determining response properties. However, we are not aware of any previous systematic study of the DOS for collective bubble oscillations.

2.4. *Excitation field*

In this study, we will focus the analysis of the response to the case in which the bubble oscillations are driven by a homogeneous pressure field. This is the case most relevant for the patterned surface experiments, in which the wavelength of the sound is much larger than the sample size. Results for spatially dependent pressure fields are in principle accessible by our analysis, but we will not explored them here.

This type of driving leads to an averaging, weighted by the susceptibility of a mode to in-phase excitation. Modes with lots of neighbouring bubbles oscillating in anti-phase are driven much less effectively than modes with more oscillations in phase. Therefore, the fact that all bubbles are driven with the *same* phase has important implications for the response (examples shown in figure 1(*b*1–*b*4)).

2.5. *The effect of viscous damping and number of bubbles on collective dynamics*

We already saw above that since the single-bubble Q-factor is large, viscous effects on single-bubble oscillations are typically small. But this is not necessarily so for collective response. In the simplest case, the Q-factor of collective modes is not very different from that of a single bubble, so that its frequency response has a width of order $1/Q$. Actually, if we excite an array of N bubbles by a frequency ω, we will only observe single-mode-like response if there are no other modes within a frequency window of order $1/Q$ around ω. In other words, we will have

$$\left.\begin{array}{l}\text{single-mode response for } ND(\omega)/Q \lesssim 1,\\ \text{multi-mode response for } ND(\omega)/Q \gtrsim 1.\end{array}\right\} \tag{2.5}$$

Clearly, even though the quality factor Q may be large, the sharpness of the individual mode resonances competes with the increase in number of modes N when the cloud gets larger. Moreover, this effect is strongly dependent on the shape of $D(\omega)$: for low frequencies, where $D(\omega)$ is found to be small, it is possible to observe single collective mode response even for reasonable values of N (e.g. mode in figure 1(*a*1) versus response in figure 1(*b*1)), but for relatively high frequencies, where $D(\omega)$ is large, it is virtually impossible to see single-mode behaviour in response (e.g. modes in figures 1 (*a*3)–1(*a*4) versus response in figures 1(*b*3)–1(*b*4)). So even though the damping itself is small, in the latter case the effect of damping is large, through the overlap of the modes. These considerations also affect the possibility to see localization effects of modes, accompanying the discussion in § 2.2.

2.6. *Polydispersity*

In experiments, bubbles have different static radii and hence have different individual-bubble resonance frequencies. This is actually the most important source of disorder in this system, because bubbles which have similar single-bubble resonances are resonantly coupled, and those which have different ones are effectively only weakly coupled. Consequently, even the introduction of polydispersity as small as a few per cent in an ordered bubble array will turn out to destroy most of the coherent collective modes of the ordered system. Note also that because of the long-range pressure-mediated interaction, bubbles which are relatively far away but which have similar single-bubble resonant frequencies can exhibit strong effective coupling. As a result, the most important factor determining the spectrum is the polydispersity of the bubbles.

As we shall see, the strongly disordered modes are mostly found at higher frequencies, where $D(\omega)$ is also large (see figures 1(a3)–1(a4)). In view of (2.5), upon driving we will typically observe multi-mode response in this frequency range. The averaging over many modes will turn out to wash out much of the disorder in the individual modes: the average response is more coherent than one might have expected, as it turns out to be concentrated at the *edges* of the sample, as shown in figure 1(b4). This pronounced response of the bubbles at the edge of the bubble cloud qualitatively resembles the experimental observations of Bremond *et al.* (2006*a*,*b*), where the phenomenon had been called 'shielding' of the inner bubbles. (Note however that in Bremond *et al.* 2006*a*, *b* the bubbles are oscillating in the nonlinear regime so that no quantitative agreement can be expected.)

In line with the above arguments, the lowest-frequency modes are those where many bubbles oscillate mostly in phase, figure 1(a1). These modes are less sensitive to the disorder, and moreover, since the low-frequency DOS is very small, these modes can be observed as isolated modes upon driving. The existence of a low-frequency collective response is qualitatively consistent with the experimental observation of Rathgen *et al.* (2007), who found the most pronounced frequency response of collectively oscillating micromenisci around 150 kHz, though the resonance of a single micromeniscus was around 800 kHz.

In this paper, we will study only bubble size distributions which are relatively well peaked, e.g. like a Gaussian distribution with a width up to 20 %, which is a typical polydispersity for e.g. ultrasound contrast agents (Burns 1996). In the experiments of Bremond *et al.* (2006*a*, *b*) a much sharper bubble size distribution is achieved.

We will refer to the case of 20 % polydispersity as 'strong polydispersity', whereas the case of 1 % polydispersity which we analyse for comparison will be referred to as 'weak polydispersity'. We have also explored bubble size distributions with power-law tails for small radii (like the Wigner distribution), as well as uniform distribution of finite width, and the obtained results are qualitatively similar to the Gaussian ones.

2.7. *Influence of geometry and geometric disorder*

The geometric disorder, e.g. due to randomness in the placement of bubbles, appears to have a relatively unimportant effect, provided that bubbles are never extremely close to each other. We in fact see little difference between various ordered bubble arrays (square, hexagonal, rhombic) and disordered bubble arrangements. This appears to be due to the long-range pressure-induced interaction, which makes the coupling quite insensitive to the details of the local geometry.

2.8. *Effect of dimensionality*

In this paper, we focus on two-dimensional bubble arrays, both because of the relevance to the recent experiments and because the modes and response are easier to illustrate in two dimensions. We already saw above that because of the long-ranged interactions, the local geometry hardly matters. All what matters in (3.1) are the relative distances of the bubbles, not the location of the bubble. Likewise, many of our results will carry over to three-dimensional arrays, but a detailed analysis of the three-dimensional problem is beyond the scope of the present paper.

2.9. *Localization*

What sets our system apart from the usual systems displaying localization effects is the long-range nature of the interaction. We do see localization-like behaviour in the individual modes in quantities like the participation ratio, especially for extremal bubbles at large polydispersity, but as we shall detail in § 5.3, due to the long-range coupling between the bubbles, there is no true exponential localization of the eigenmodes (as already mentioned in § 2.2). Localization effects that we observe play a limited role in the response: these modes are mostly found in a frequency range where multi-mode averaging already washes out many of the disorder effects on individual modes.

3. Oscillations of the bubbles

3.1. *Extended Rayleigh–Plesset equation with driving*

The dynamics of interacting bubbles in a cluster can be described with the extended Rayleigh–Plesset equation (see e.g. Doinikov 2004; Pelekasis *et al.* 2004; Mettin 2005; Bremond *et al.* 2006*a*,*b*)

$$R_i\ddot{R}_i+\frac{3}{2}\dot{R}_i^2=\frac{1}{\rho}\left[\left(p_0^\infty+\frac{2\sigma}{R_i^0}-p_v\right)\left(\frac{R_i^0}{R_i}\right)^{3\kappa}-\frac{2\sigma}{R_i}+p_v-4\mu\frac{\dot{R}_i}{R_i}-(p_0^\infty-P_a\cos(\omega_d t))\right]-\sum_{j\neq i}\frac{R_j^2\ddot{R}_j+2R_j\dot{R}_j^2}{r_{ij}},\quad(3.1)$$

where $R_i(t)$ is the radius of the ith bubble and R_i^0 its static value, ρ is the density of the surrounding liquid, σ is the surface tension, μ is the viscosity, p_0^∞ is the ambient pressure, p_v is the vapour pressure, P_a is the driving pressure amplitude, ω_d is the driving frequency, and r_{ij} the distance between the centre of the ith and the jth bubble. Since the sizes of the bubbles we are going to treat in this study are small (of the order of a few μm) compared to the thermal diffusion length on the oscillation time scales, we will assume that the gas inside the bubble follows an ideal gas law, modelled with the polytropic coefficient $\kappa=1$ (Plesset & Prosperetti 1977; Hilgenfeldt, Lohse & Brenner 1996). This isothermal assumption is justified (Prosperetti 1977; Crum 1983; Kamath, Prosperetti & Egolfopoulos 1993; Brenner *et al.* 2002) as the Peclet number $Pe=\omega_d R_0^2/(2\pi\chi_g)$ for the process of bubble oscillation is only about 0.05 for the 5 μm bubbles driven at $\omega/2\pi\approx 20$ kHz considered in the paper. Here, χ_g is the thermal diffusivity of the gas. Finally, for simplicity we will neglect the pressure of the liquid vapour (for water at 20 °C, it is only 0.023 atm).

Note that in the last term in (3.1), which models the bubble–bubble interaction mediated by the pressure, we have included only the leading term of order R/r. This is of course only quantitatively accurate when bubbles are not too close to each other. Inclusion of higher-order interaction terms is numerically straightforward but is not

expected to significantly change the qualitative behaviour, in particular for ordered arrays and for the lowest-frequency in-phase modes (for these the higher-order terms mostly affect the effective strength of the interaction).

Likewise, in (3.1) the fluid is treated as incompressible. This is justified for the frequencies and spatial scales used in experiments. In our model, compressibility would add a distance-dependent phase shift to the interaction term. As long as the frequencies are small enough (i.e. $\omega \ll c/r_{ij}$, where $c \approx 1480$ m s^{-1} is the speed of sound in water) so that the phase shift between neighbouring bubbles remains small, the effect will again not affect the qualitative behaviour very much. As the phase shift increases, the low-frequency in-phase mode that we generally find in the analysis below will turn into a modulated mode that follows the propagation of the pressure field along the bubble array. The higher-frequency modes with many out-of-phase oscillations will then change character dramatically. Moreover, as we shall see in § 5.3, where we do include the phase factor coming from compressibility, a finite compressibility does change the power-law localization into an exponential localization.

3.1.1. *Small driving limit*

In the limit of small driving, $P_a \ll p_0^\infty$, (3.1) can be linearized about the static values R_i^0 (as long as $P_a/p_0^\infty \leqslant 0.2$, this is clearly satisfied). As motivated in the introduction, in the analysis of this paper we will restrict ourselves to this limit. The linearization results in a set of coupled damped linear oscillators (Hilgenfeldt *et al.* 1998). Switching to dimensionless variables by substituting $R_i = R_i^0(1+q_i)$ into (3.1), we get

$$\ddot{\tilde{q}}_i(t) + \sum_{j\neq i} \frac{\sqrt{R_j^0 R_i^0}}{r_{ij}} \ddot{\tilde{q}}_j(t) + \frac{4\mu}{\rho\left(R_i^0\right)^2}\dot{\tilde{q}}_i(t) + \left(\Omega_i^0\right)^2 \tilde{q}_i(t) = \frac{P_a}{\rho\left(R_i^0\right)^2}\left(\frac{R_i^0}{\langle R_i^0\rangle}\right)^{1/2}\cos(\omega_d t), \tag{3.2}$$

where $\tilde{q}_i(t) = (R_i^0/\langle R_i^0\rangle)^{5/2} q_i(t)$ is a rescaled displacement of the ith bubble to make the equation symmetric in the bubble indices i and j, and ω_d is a driving frequency (after substituting $R_i = R_i^0(1+q_i)$ into (3.1) and keeping linear terms only, one is left with an equation that is not symmetric under the change of indices i and j due to the coupling term; simple rescaling of the displacements makes the relevant $\boldsymbol{C}$ matrix (see below) symmetric and therefore the eigenvalue problem easier). The brackets $\langle\cdot\rangle$ denote an average over the bubble size distribution. We also used the fact that

$$(\Omega_i^0)^2 = \frac{3p_0^\infty}{\rho\left(R_i^0\right)^2} + \frac{4\sigma}{\rho\left(R_i^0\right)^3} \tag{3.3}$$

is simply the (squared) single-bubble resonance frequency, i.e. the resonance frequency of each individual bubble i in the absence of damping and of interactions with any of the other bubbles. This equation generalizes (2.1) given in the introduction; as remarked there, the surface tension term is small for bubbles of radius larger than several μm.

Equation (3.2) is the linearized Rayleigh–Plesset equation with damping, coupling and driving that is the starting point for our calculations. For simplicity, we can rewrite (3.2) in a matrix form,

$$\boldsymbol{C}|\ddot{\tilde{q}}(t)\rangle + \boldsymbol{\zeta}|\dot{\tilde{q}}(t)\rangle + \boldsymbol{\Omega}|\tilde{q}(t)\rangle = |P\rangle \exp(-\imath\omega_d t), \tag{3.4}$$

where we used a quantum mechanics-like notation $|\tilde{q}\rangle$ for the vector that contains all the individual displacements $\tilde{q}_i$ of the bubbles. $\boldsymbol{C}$ is a symmetric coupling matrix

that has diagonal elements $[\boldsymbol{C}]_{ii}$ equal to 1 and off-diagonal elements $[\boldsymbol{C}]_{ij}$ equal to $\sqrt{R_i^0 R_j^0}/r_{ij}$. $\boldsymbol{\zeta}$ is a diagonal friction matrix with elements $[\boldsymbol{\zeta}]_{ii} = 4\mu/(R_i^0)^2\,\rho$, while the matrix $\boldsymbol{\Omega}$ is a diagonal matrix whose elements are simply the square of the single-bubble resonant frequencies, $[\boldsymbol{\Omega}]_{ii} = \Omega_i^2$. The driving term on the right-hand side is the vector $|P\rangle$ whose elements are $P_i = P_a/(\rho(R_i^0)^2)\cdot(R_i^0/\langle R_i^0\rangle)^{1/2}$. Depending on the presence of polydispersity in our system, the approach to solving the matrix equation (3.4) numerically differs. Therefore we will address each case separately.

3.2. *Spectrum of the system*

3.2.1. *Monodisperse system*

When the initial bubble sizes are the same, $\boldsymbol{\zeta} = \zeta\mathbf{1}$, $\boldsymbol{\Omega} = \Omega_0^2\mathbf{1}$, where $\mathbf{1}$ is the identity matrix and P_i is the same for all the bubbles. To find all the resonant frequencies of the system, we need to solve the homogeneous equation, without the driving term. We assume a solution of the form $|\tilde{q}(t)\rangle = |u\rangle\exp(-\imath\omega t)$, where $|u\rangle$ is the displacement vector and ω is the oscillation frequency of the system. Substituting this solution into (3.4) without the driving term, we can rewrite the equation in the eigenvalue form:

$$\boldsymbol{C}|u\rangle = \left(\frac{\Omega_0^2 - \imath\omega\zeta}{\omega^2}\right)\mathbf{1}|u\rangle. \tag{3.5}$$

Let us first consider the eigenvalue equation without the damping (i.e. $\zeta = 0$), and denote its eigenvalues by λ_i, i.e. $\boldsymbol{C}|u_i\rangle = \lambda_i|u_i\rangle$. The eigenvalues of the coupling matrix $\boldsymbol{C}$ are real and related to the eigenfrequencies of the undamped system $\tilde{\omega}_i$ as $\lambda_i = \Omega_0^2/\tilde{\omega}_i^2$. Eigenvectors (or eigenmodes) $|u_i\rangle$ corresponding to λ_i are also real, which means that all the bubbles oscillate either in phase or in anti-phase (corresponding to a phase difference of π). From (3.5) we see that these eigenmodes are also the eigenmodes of the damped case where $\zeta \neq 0$ (this is valid only for monodisperse systems), while the eigenfrequencies become complex:

$$\omega_i^{\pm} = -\frac{\imath\zeta\tilde{\omega}_i^2}{\Omega_0^2} \pm \frac{\tilde{\omega}_i\sqrt{4\Omega_0^4 - \zeta^2\tilde{\omega}_i^2}}{2\Omega_0^2}. \tag{3.6}$$

The real part of this solution corresponds to the resonant frequency of the mode, and the imaginary part is the damping of the resonance (widths of the Lorentzians, $1/Q$). We choose the positive solutions ω_i^+ for the resonant eigenfrequencies of the damped system. (We note in passing that it is easy to work out the above equations by hand for the instructive case of a system of two bubbles. In this case the matrix $\boldsymbol{C}$ has off-diagonal terms due to the pressure coupling. One finds a lower-frequency in-phase mode and a higher-frequency anti-phase mode, which demonstrates a general observation of § 1.)

In general, the eigenmodes $|u_i\rangle$ are complex vectors, and the imaginary part describes the phases with which bubbles oscillate. Only in the case of monodisperse bubbles, $\mathrm{Im}(|u_i\rangle) \equiv 0$ and consequently bubbles oscillate in phase or anti-phase.

3.2.2. *Polydisperse system*

In the case when the static bubble radii R_i are not the same, i.e. $R_i^0 \neq R_j^0$, the equation of motion for the system becomes more complicated to solve. In cases like these it is numerically convenient to go to (larger) phase space and search for the solution there. Equation (3.4) without the driving term will be rewritten in the following way:

$$\tilde{\boldsymbol{C}}\dot{\boldsymbol{y}} + \tilde{\boldsymbol{\Omega}}\boldsymbol{y} = 0, \tag{3.7}$$

where

$$\boldsymbol{y} = \begin{bmatrix} \dot{\tilde{q}} \\ \tilde{q} \end{bmatrix}_{2N\times 1}; \quad \tilde{\boldsymbol{C}} = \begin{bmatrix} 0 & \boldsymbol{C} \\ \boldsymbol{C} & \zeta \end{bmatrix}_{2N\times 2N}; \quad \tilde{\boldsymbol{\Omega}} = \begin{bmatrix} -\boldsymbol{C} & 0 \\ 0 & \boldsymbol{\Omega} \end{bmatrix}_{2N\times 2N}. \tag{3.8}$$

The new variable $\boldsymbol{y}$ is a vector in the phase space formed out of the degrees of freedom $\tilde{q}$ and their velocities $\dot{\tilde{q}}$. A solution has the form $\boldsymbol{y} = \boldsymbol{\Phi} e^{-\gamma t}$, where the set $\{\gamma_i\}$ is the $2N$ eigenvalues of $\tilde{\boldsymbol{C}}^{-1}\tilde{\boldsymbol{\Omega}}$, and the corresponding (complex) eigenvectors $\{\boldsymbol{\Phi}_i\}$ satisfy the orthogonality relation $\boldsymbol{\Phi}_i^T \tilde{\boldsymbol{C}} \boldsymbol{\Phi}_j = 0$, for $i \neq j$. Since $\dot{\boldsymbol{y}} = -\tilde{\boldsymbol{C}}^{-1}\tilde{\boldsymbol{\Omega}}\boldsymbol{y}$, we again arrive at the familiar eigenvalue problem

$$\tilde{\boldsymbol{C}}^{-1}\tilde{\boldsymbol{\Omega}} \begin{bmatrix} \boldsymbol{\Phi}^{(1)} \\ \boldsymbol{\Phi}^{(2)} \end{bmatrix} = \gamma \begin{bmatrix} \boldsymbol{\Phi}^{(1)} \\ \boldsymbol{\Phi}^{(2)} \end{bmatrix}, \tag{3.9}$$

where $|\Phi_i^{(1)}\rangle$ ($|\Phi_i^{(2)}\rangle$) are the first (last) N components of an eigenvector Φ_i, with $|\Phi_i^{(1)}\rangle = -\gamma_i |\Phi_i^{(2)}\rangle$. The imaginary parts of the eigenvalues $\{\gamma_i\}$ are the resonant frequencies, and the real parts are the damping rates. The eigenvalues $\{\gamma_i\}$ are always paired into complex conjugate values, so out of $2N$ values, we select N with positive resonant frequencies, which together with the corresponding eigenvectors $|\Phi_i^{(2)}\rangle$ compose the desired N-dimensional solution of the problem. The formalism presented in this subsection can, of course, also be used for treating the monodisperse systems. The only advantage of the monodisperse approach, described in § 3.2.1, is the dimensionality of the solution space: instead of searching for N solutions in $2N$-dimensional space, we are searching it in N-dimensional space.

3.3. *Response of the system to harmonic driving*

3.3.1. *Driving of the monodisperse system*

We are interested in the long-time limit response of the system when driven with a real frequency ω_d. The following formulae are valid for arbitrary real frequency ω_d, although in most of our presented results, we will set ω_d to the resonant frequencies of the system.

We proceed by substituting the solution $|\tilde{q}\rangle = |W\rangle e^{-\imath\omega_d^i t}$ into (3.4), which then gives

$$\left(-{\omega_d^i}^2 \boldsymbol{C} - \imath\omega_d^i \zeta \mathbf{1} + \Omega_0^2 \mathbf{1}\right)|W\rangle \equiv \Xi |W\rangle = |P\rangle. \tag{3.10}$$

To find the response vector, we can act on the driving amplitude vector with Ξ^{-1}. For every driving frequency, we have $|W(\omega_d^i)\rangle$ and these vectors are complex because of the presence of damping. The response of the system written in terms of the eigenvectors of the undriven system is

$$|W(\omega_d^i)\rangle = \sum_{j=1}^{N} \frac{\langle u_j | P\rangle}{-{\omega_d^i}^2\left(\Omega_0^2/\tilde{\omega}_i^2\right) - \imath\omega_d^i\zeta + \Omega_0^2} |u_j\rangle, \tag{3.11}$$

where ω_d^i is one of the resonant frequencies ω_i calculated in § 3.2.1, and $\tilde{\omega}_i$ is the corresponding eigenfrequency of an undamped system. According to this equation, the response of the system can be thought of in terms of the sum of many independent damped harmonic oscillators (the modes), each of which has a response given by the factor in the denominator. This is precisely the picture which underlies the discussion in § 2.5 of the distinction between the single-mode response and the multi-mode response. Moreover, the extent to which each mode is excited is given by the overlap $\langle u_i | P\rangle$; as discussed below, we will refer to it as the 'excitability' of a mode. Since $|P\rangle$ is a vector with only positive items, this excitability is largest for the modes where all

bubbles oscillate in phase and zero for perfectly antisymmetric modes. Compare the discussion in § 2.4.

3.3.2. *Driving of the polydisperse system*

We now apply the driving $\tilde{P}(t)$ to the coupled polydisperse bubble system (3.7):

$$\tilde{\mathbf{C}}\dot{\mathbf{y}} + \tilde{\boldsymbol{\Omega}}\,\mathbf{y} = \tilde{P}, \quad \text{where } \tilde{P}(t) = \begin{bmatrix} 0 \\ P(t) \end{bmatrix}. \tag{3.12}$$

To find the response, we need to go to the undriven eigenbasis. The calculation is tedious, but the final form is a straightforward generalization of (3.11) for the monodisperse case:

$$|W(\omega_d^i)\rangle = \sum_{j=1}^{N} \frac{\langle \Phi_j^{(2)}|P\rangle}{\gamma_j - \imath\omega_d^i}|\Phi_j^{(2)}\rangle. \tag{3.13}$$

As already mentioned above, it is convenient to introduce the *mode excitability* in connection with the driving – it describes the overlap between an eigenmode $|u_i\rangle$ of the system ($|\Phi_i^{(2)}\rangle$ for the polydisperse system) and the driving amplitude vector $|P\rangle$, i.e. $\chi_M^i = \langle u_i|P\rangle$ ($\chi_M^i = \langle \Phi_i^{(2)}|P\rangle$). This quantity states whether an eigenmode can be excited when the system is driven with a certain resonant frequency. One should keep in mind, however, that the weight of an eigenmode in the response is also determined by the resonance curve factor (e.g. (3.11)) and by the interference between modes. We will also present the *response excitability*, which represents the overlap between the response vector and the driving amplitude $\chi_R^i = \langle W(\omega_d^i)|P\rangle$, as well as the *absorption*, which is defined as the average dissipated energy during one period T of driven oscillation, $T^{-1}\int_0^T \mathrm{d}t \sum_i P(t)\dot{\tilde{q}}_i(t)$, where $P(t)$ is the force exerted on the system and $\tilde{q}_i(t)$ are the instantaneous bubble displacements. Absorption is given by the imaginary part of the overlap of the response and driving vectors, i.e. the absorption $\sim T^{-1}\int_0^T \mathrm{d}t\,\mathrm{Re}(\langle P|\mathrm{e}^{\imath\omega t}\rangle\mathrm{Re}(|W\rangle) = (\omega/2\pi)\,\mathrm{Im}(\langle P|W\rangle)$. To be able to better relate to the experiments, we will also calculate the *frequency response* ϵ_R, defined as $|W(\omega_d)|^2$.

3.4. *Localization of vibrations*

We will now explore the localization behaviour of the eigenvectors of the system and of the response to driving. A standard way to explore this is by looking at the behaviour of the so-called participation ratio $P(\omega)$, which is defined as follows:

$$P(\omega_i) = \frac{1}{N}\frac{\left(\sum_j |v_i^j|^2\right)^2}{\sum_j |v_i^j|^4}. \tag{3.14}$$

Here the $|v_i\rangle$ are either the eigenmodes $|u_i\rangle$ of the system ($|\Phi_i^{(2)}\rangle$ for the polydisperse system) or the response vectors $|W(\omega_d^i)\rangle$, giving the *mode participation ratio*, $P_M(\omega_i)$, or the *response participation ratio*, $P_R(\omega_d^i)$, respectively. If P_M (P_R) is of order 1, it means that the mode (response) is extended, and if it is of order $1/N$, the mode (response) is normally called localized. However, we will later show that due to the long-ranged interactions, this picture is over-simplified.

4. Results: monodisperse bubbles on a lattice

Although in experiments bubble polydispersity is always present, in the interest of developing intuition about the system we first consider an 'idealized' case of monodisperse bubbles on a lattice.

4.1. *Undriven system*

As explained in § 1, we perform numerical simulations of clusters of bubbles, whose dynamics is described with the linearized extended Rayleigh–Plesset equation (3.2). Most of the presented results are for system sizes $N \sim 1000$ bubbles in 2D. We study some of the behaviour for system sizes $N \sim 10\ 000$ to check for finite size effects. Parameters that we use in simulations are as follows: *effective viscosity* $\mu = 2\times10^{-3}$ Pa s (by effective we mean that we also account for thermal damping, as often done for Rayleigh–Plesset dynamics without a coupling to the temperature field, see e.g. the textbook by Brennen (1995) or the reviews by Plesset & Prosperetti (1977) and Brenner *et al.* (2002); the factor 2 as compared to the viscosity of water was taken from van der Meer *et al.* (2007)), *density of water* $\rho = 10^3$ kg m^{-3}, *surface tension* $\sigma = 0.073$ N m^{-1}, *atmospheric pressure* $p_{atm} = 101.325$ kPa, *driving amplitude* $P_a = 20.265$ kPa, *static bubble radius* $R_0 \approx 5\,\mu$m and *pitch* $d = 200\,\mu$m, and we explore three different geometries: *rhombic, square and hexagonal*. With these parameters, (3.3) gives a single-bubble resonant frequency $\Omega_0 \approx 4\times10^6$ rad s^{-1}. Frequencies will be plotted in units of Ω_0. The corresponding values of the sharpness of the resonances Q, defined in (2.3), and the interaction parameter K, defined in (2.4), are then $Q_0 \simeq 25$ and $K_0 = 1/40$ (we label these reference values with a subscript 0). These quantities will be different when we consider polydisperse systems in § 5.

4.1.1. *Spectrum*

Starting from (3.4), we solve the undriven eigenvalue problem and obtain eigenmodes and eigenvalues. A few of the obtained eigenmodes (from different parts of the spectrum) are shown in figure 2. The size of the bubbles is proportional to the amplitude of the oscillation and the colour shows the phase. Note how, in agreement with the earlier analysis in § 3.2.1, in the eigenmodes bubbles oscillate either in phase or in anti-phase, giving the modes their plane-wave-like structure. Although different arrangements of the bubbles (rhombic, hexagonal, etc.) naturally have different symmetry axes, the general features of the mode profile remain robust, as already indicated in § 2.7.

A histogram of the resonant frequencies (real parts of the eigenvalues), i.e. the DOS (see § 2.3), for different system sizes in rhombic geometry is shown in figure 3(*a*) in a semi-logarithmic scale. The DOS is significantly denser around the single-bubble resonant frequency. As in Rathgen *et al.* (2007), we also observe resonant frequencies much lower in the spectrum, whose origin lies in the acoustic coupling of the bubbles. Some of these collective low-frequency modes are depicted in figure 2(*a–c*). The arrows in figure 3(*a*) mark the crossover from the single-mode behaviour ($N D(\omega)/Q \lesssim 1$) at low frequencies to the multi-mode response at higher frequencies. Clearly, for these parameters only one or a few isolated low-frequency modes can be observed in response.

Figure 3(*b*) shows the finite size effects for the lowest-frequency mode, where all bubbles oscillate in phase, and the mode is of course of the size of the system. It is damped the least and scales with the system size as $\omega^2_{lowest} \sim 1/L = 1/N^{1/2}$, where L is the linear system size and N is the number of bubbles. This behaviour is different from the usual $\omega^2_{lowest} \sim 1/L^2$ scaling in systems described by the wave

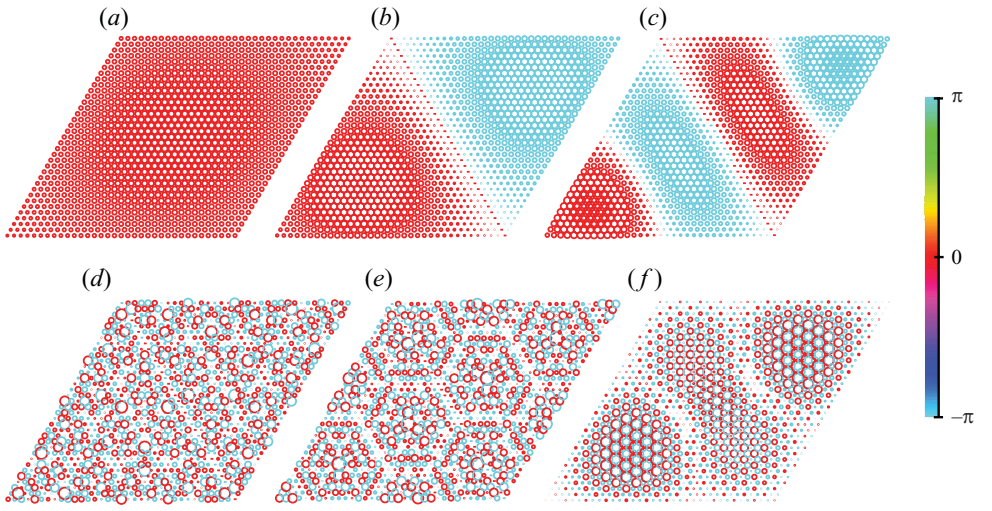

FIGURE 2. (Colour online) Six eigenmodes of the undriven monodisperse 2D bubble cluster. For this illustration we chose (*a–f*) the 1st ($\omega/\Omega_0 \approx 0.54$), 3rd ($\omega/\Omega_0 \approx 0.74$), 5th ($\omega/\Omega_0 \approx 0.80$), 9th ($\omega/\Omega_0 \approx 0.84$), 1128th ($\omega/\Omega_0 \approx 1.01$) and 1218th ($\omega/\Omega_0 \approx 1.02$) modes of the system with 1225 bubbles in rhombic geometry. The radii of the circles in the plot are proportional to the amplitude of the oscillation and the colour shows the phase. Note how in the eigenmodes bubbles oscillate either in phase or in anti-phase.

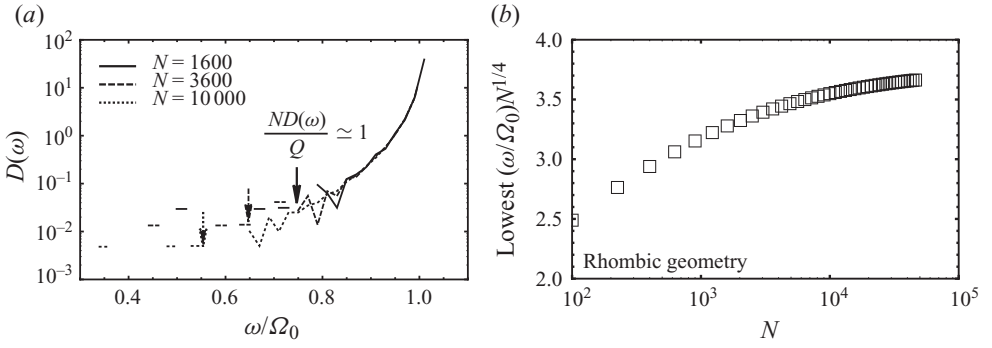

FIGURE 3. (*a*) DOS for the 2D monodisperse bubble cluster in rhombic geometry on a log-linear scale. Different curves represent different system sizes. Note the pronounced peak in the spectrum at the single-bubble resonant frequency. As mentioned in § 1, due to the coupling between the modes, there are resonant frequencies in the spectrum lower than the single-bubble one. The arrows mark the value in the DOS, where the response changes from single-mode to multi-mode (as defined in § 2.5). (*b*) Scaling of the lowest-frequency mode with the increase of the system size. The value of the lowest frequency is rescaled with $N^{1/4}$ to emphasize the asymptotic approach to a constant value in the thermodynamic limit.

equation and originates in the long-range interaction of the bubbles in a cluster. The way to understand this scaling is as follows: starting from (3.5), in which we can ignore the damping, and noting that the lowest mode $|u_0\rangle$ is approximately uniform, we see that in the large-N limit $\mathbf{C}|u_0\rangle = \sum_j C_{ij} u_0^j \to \int_S \mathrm{d}\boldsymbol{r}\ C_{ij} u_0^j \equiv \Omega_0^2/\omega_{lowest}^2$, and the scaling structure of the equation is such that $\omega_{lowest}^2 \int_0^L r\,\mathrm{d}r (R_0/r) \sim \omega_{lowest}^2 L \sim \Omega_0^2$. Hence, $\omega_{lowest} \sim L^{-1/2} \sim N^{-1/4}$. To emphasize the finite size effects, we rescale the lowest frequency with $N^{1/4}$ in this figure. Note that systems with $N \sim 1000$ are large

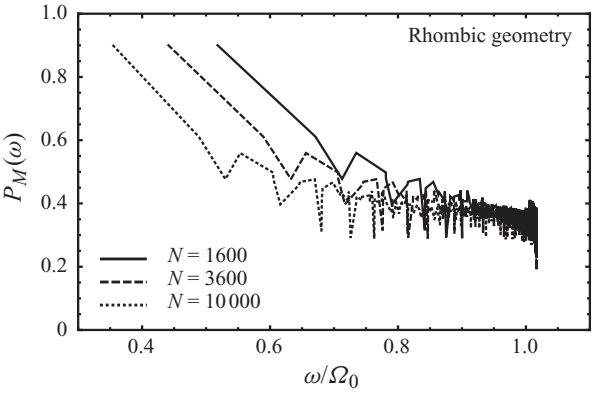

FIGURE 4. Participation ratio of the eigenmodes as a function of the rescaled resonant frequency. Data points are joined by lines for clarity. Different curves represent different system sizes, and the geometry we use is rhombic. Eigenmodes of the monodisperse system are the collective plane-wave-like modes that span the system and are of extended nature.

enough to capture the essential behaviour of the bubble clusters. As in the case of modes, the geometry does not play a significant role (see also § 2.7).

4.1.2. *Mode participation ratio*

Examples of the eigenmodes presented in figure 2 indicate an extended nature (they are spanning the system). To quantify this behaviour, for every eigenmode we calculated the participation ratio defined in § 3.4. This result is shown in figure 4 for different system sizes and rhombic geometry at the resonant frequency of each mode. Except for the lowest-frequency modes, that are extended throughout the system ($P_M(\omega) \sim 1$), the rest of the modes form a plateau with an average $P_M(\omega) \sim 0.4$. In this idealized case of monodisperse bubble clusters, there are no truly localized eigenmodes (modes where the motion is localized on a single bubble or a small group of bubbles), but only plane-wave-like collective modes. This behaviour is independent of the geometry of the problem.

4.2. *Driven system*

As stated in § 2.5, the analysis of the response to driving presents an unexpected effect, namely the *effective damping*, which washes out features in the response. In this subsection we present additional details and results.

4.2.1. *Response participation ratio and response excitability*

A few characteristic examples of the response of the system to uniform driving with resonant frequencies (equation (3.11)) are shown in figure 5. Except for the first few responses (driving with the lowest frequencies) that have plane-wave-like structure (figure 5(*a–c*)), the rest of the response patterns are similar and dominate at the system boundaries (representatives shown in figure 5(*d–e*)). This property is also clearly measured by the participation ratio of the response vectors, shown in figure 6(*a*) for three different system sizes and rhombic geometry. Namely, for most of the driving frequencies in the spectrum, the response participation ratio defined in § 3.4 is $P_R(\omega) \lesssim 0.3$ and decreases with increasing system size, indicating a boundary confinement. (Obviously, these are not localized responses in the sense of Anderson localization, i.e. due to disorder, but are corresponding to edge states in finite systems.)

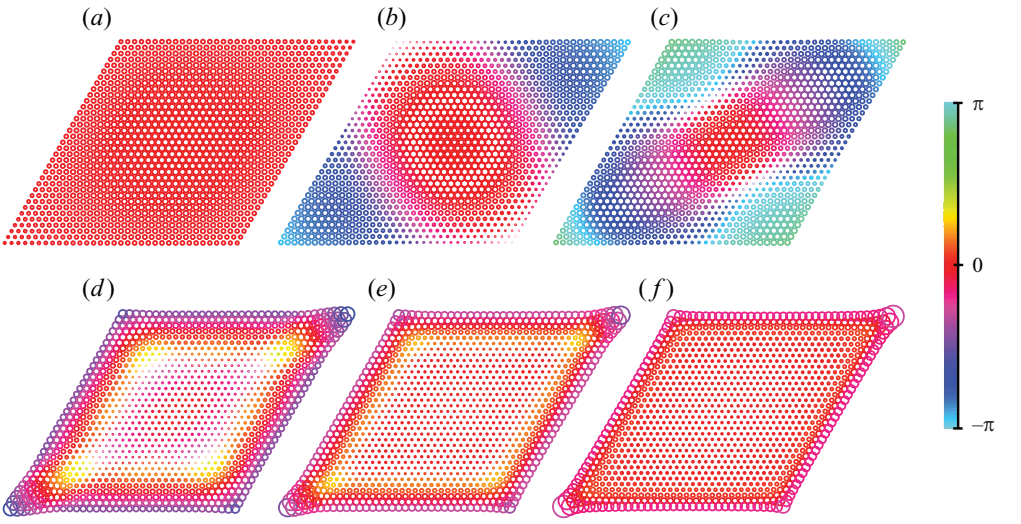

FIGURE 5. (Colour online) Response of the monodisperse 2D cluster of 1225 bubbles, when driven with (*a–f*) the 1st ($\omega_d/\Omega_0 \approx 0.54$), 3rd ($\omega_d/\Omega_0 \approx 0.74$), 5th ($\omega_d/\Omega_0 \approx 0.80$), 50th ($\omega_d/\Omega_0 \approx 0.94$), 107th ($\omega_d/\Omega_0 \approx 0.97$) and 1107th ($\omega_d/\Omega_0 \approx 1.02$) resonant frequencies. The radii of the circles around the bubble locations are proportional to the amplitude of the oscillation and the colour shows the phase. Note how the response fields are featureless for driving above the lowest eigenfrequencies, both because of the overlap of many modes which washes out single-mode effects and because modes with strong out-of-phase oscillations couple weakly to the uniform pressure driving, as discussed in §§ 2.4 and 2.5.

The thickness of the boundary layer monotonically decreases with rising ω_d. This is clearly visible also in figures 5(*d*)–5(*f*).

Figures 5(*d*)–5(*f*) indicate an important clue for understanding the nature of these response fields. One can see that the majority of bubbles oscillate almost in phase with the driving. This leads to a resemblance between the response and the uniform driving field, as captured by the upswing in the *response excitability*, figure 6(*b*) (introduced in § 3.3.2). We find this behaviour to be robust to introducing disorder. It is intriguing that in the experiments of Bremond *et al.* (2006*b*), the observed oscillations resemble the low- and high-frequency response fields (the ones with high $\chi_R(\omega)$).

4.2.2. *Mode excitability and contributions*

We interpret the absence of extreme sensitivity on ω as it is seen in the mode participation ratio (cf. figure 2) and the almost in-phase oscillation as a consequence of the excitation of many modes (as $ND(\omega)Q \gg 1$, see the explanation in § 2.5). To illustrate this point, we analyse the eigenmode content of the response fields. According to (3.11), the eigenmode enters the response weighed by two factors: (*i*) the mode excitability (defined in § 3.3.2) and (*ii*) its Lorentzian (i.e. the mode resonance curve) evaluated at the driving frequency. The normalized value of the first factor rapidly decays towards zero across the spectrum, except for the lowest mode for which it is normalized to 1, figure 7(*a*) (note that due to the symmetry, half of the modes are antisymmetric and therefore have zero excitability). However, the resonance factor controlled by the mode Q-factor (see § 2.1) singles out modes closest to the driving frequency. The final contribution of the eigenmodes is determined by an interplay of these two numbers; we plot characteristic outcomes in figure 7(*b*1–*b*4).

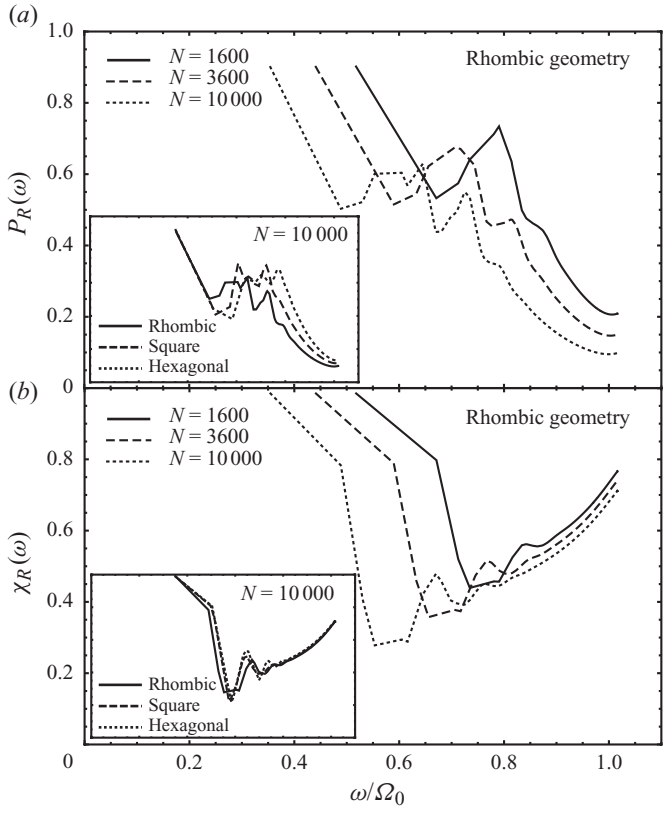

FIGURE 6. (*a*) Participation ratio of the response versus scaled driving frequency for three different system sizes and rhombic geometry. Apparently localized response corresponding to driving with high-frequency modes is actually an edge response restricted to the system boundaries. The inset shows the robustness of the behaviour of $P_R(\omega)$ to the change of the geometry. (*b*) Response excitability versus scaled driving frequency for different cases as in (*a*). The response field resembles the uniform driving amplitude when the system is driven with the lowest-frequency mode or with the modes at the high end of the spectrum. The inset shows the robustness to geometry change. In both (*a*) and (*b*), data points are connected with lines for clarity.

Due to its excitability, the lowest mode always contributes significantly, figure 7(*b*1–*b*4). However, the striking result is that since the density of modes is large (except for a few lowest, the rest $\sim N$ eigenmodes are clustered around the single-bubble resonant frequency, figure 3(*a*)), the single-mode resonance width (i.e. the inverse Q-factor of the mode) is always large enough to allow many modes in the vicinity of ω_d to be excited (as already seen in §§ 2.1 and 2.5). This effect leads to the cancellation of the detailed features of eigenmodes and to the 'multi-mode' synchronized oscillation of bubbles in the response field. Figure 7(*b*4) is a representative case, where the driving frequency falls inside the densest region of the DOS, leading essentially to excitation of all the modes.

In terms of the sharpness of collective resonances (introduced in § 2.5) and the mode density, the resonance width $D(\omega)/Q \sim D(\omega)\mu/\langle R_0 \rangle$ basically needs to be $\lesssim 1/N$ for individual modes to be seen. In the data presented so far, we did not include results with varying Q-factor (i.e. bubble radii or viscosity) or interaction parameter K (i.e. bubble radii or pitch). Indeed, the focus of this section was on varying system size

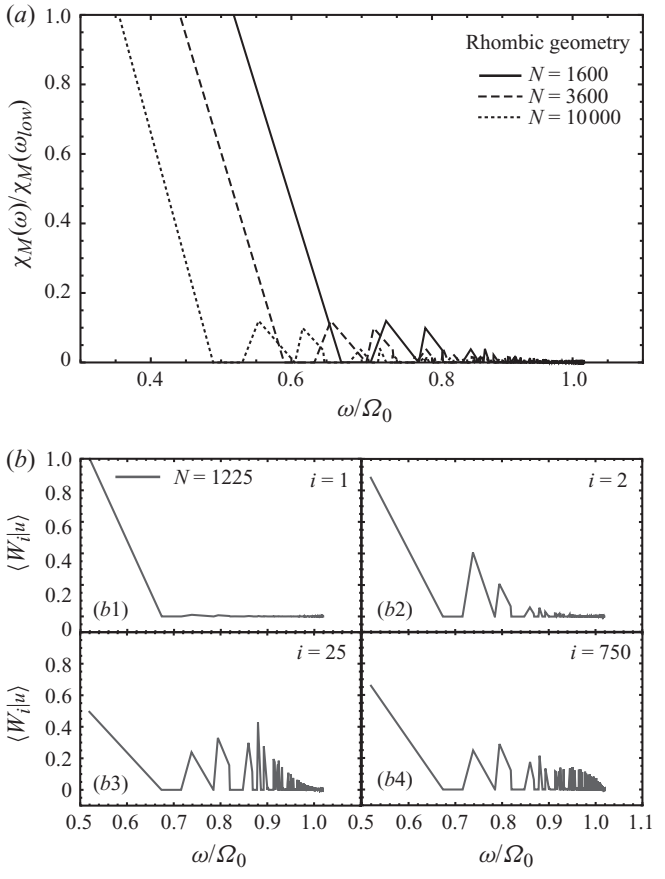

FIGURE 7. (*a*) Excitability of eigenmodes, normalized by the value for the lowest mode for three different system sizes and rhombic geometry. Note that for clarity the data points between resonant frequencies have been connected by straight lines. Due to the symmetry, only half of the modes can be excited. Except for the lowest mode that resembles the driving amplitude, the excitability of the rest of the modes falls to zero quickly across the spectrum. This behaviour is robust to the change of the geometry (not shown here). (*b*: *b*1–*b*4) Eigenmode contributions to the typical responses for a system of $N = 1225$ bubbles and rhombic geometry. Considerable contribution of the lowest eigenmode is present in every response. When the system is driven with a frequency within the densest region of the DOS in figure 3(*a*), many modes with resonant frequencies close to this value contribute almost equally to the response (*b*4).

and geometry, since the formalism presented in § 3 is numerically simpler for the case of monodisperse bubbles, allowing us to study large systems and finite size effects. We will vary Q and K for the more experimentally relevant case of disordered clusters in the next section.

5. Results: polydisperse bubbles on a lattice

After gaining understanding of the behaviour of the 'ideal' monodisperse case in the previous section, we can proceed with introducing disorder into the system. As explained in the introduction, the experimental parameter space is vast. The system is most sensitive to the changes of polydispersity of static bubble radii (§ 2.6), the sharpness of collective resonances (§ 2.1 and § 2.5) and the interaction parameter (§ 2.2). In this section we vary these parameters.

5.1. *Weak disorder*

To get an intuition of what happens to the spectrum of the 2D bubble cluster when we introduce polydispersity, we first draw static bubble radii from a Gaussian distribution with a small width of 1 %. To be able to compare the results with the ones of the monodisperse case, the Gaussian distribution is centred around the parameters we have used in the previous section, namely the ambient radius $R_0 = 5\,\mu\text{m}$ and the bubble distance $d = 200\,\mu\text{m}$. All other parameters are fixed at the values in the previous sections. Besides introducing polydispersity, we will also vary Q and K, through varying the aforementioned parameters, and express them in the units of $Q_0 \sim R_0^{mono}/\mu^{mono}$ and $K_0 \sim R_0^{mono}/d^{mono}$. The data presented in this subsection are for systems of $N = 1225$ bubbles.

5.1.1. *Spectrum and response*

The main effect on the properties of the system, when disorder is introduced, is the appearance of (quasi-)localized eigenmodes at the high-frequency end of the spectrum, figure 8(*b*) (black-dashed curve). An example of a quasi-localized mode is given in figure 8(*b*ii) – from here on, we refer to panels illustrating examples of eigenmodes or response as figure 8(ii), etc. The value of 1 % polydispersity is enough to localize a significant fraction of the eigenmodes. These quasi-localized modes have amplitudes concentrated on a group of bubbles, with some resemblance to the coherent waves of the monodisperse system.

At this point we can compare the influence of the three control parameters on the DOS. Compared to the monodisperse case, figure 8(*a*) (black solid line), introducing the polydispersity broadens the DOS, figure 8(*a*) (black-dashed line). The broadening is accompanied with a shift of the peak position towards frequencies below Ω_0 (this will become more obvious with the increase of polydispersity in the next subsection, figure 12(*a*)).

The Q-factor, i.e. the width of the collective resonances, is not expected to influence the spectrum, i.e. the positions of the collective resonances as long as Q is large. Indeed, a fivefold change of the Q-factor through the increase of $\langle R_0 \rangle$ (with K kept constant by the corresponding change of pitch d) introduces a negligible broadening of the DOS peak, which we therefore do not plot. (However, the Q-factor will become crucial for response.)

The increase of the interaction parameter K tends to shift the peak to higher frequencies while significantly broadening it, figure 8(*a*) (dash-dotted and solid lines). The stiffening of the oscillators is due to the increased interaction strength, see also § 2.2. Another consequence of the stiffening is the suppression of the localized eigenmodes at the high end of the spectrum, figure 8(*b*) (dot-dashed and solid grey lines) and the mode depicted in figure 8(iii).

The response fields strongly resemble the monodisperse case, with a mostly featureless edge character for driving at frequencies within the peak of the DOS (figure 9(ii)), and a plane-wave-like shape for low-frequency driving. The presence of disorder manifests itself in slight random spatial variation of the bubble oscillation phase in the response. Although the high-frequency eigenmodes are progressively more localized towards the spectrum edge, the DOS remains high enough for effective damping to wash out the features of the response to even the highest-frequency driving.

Following the discussions in § 2.5 and at the end of the previous section, we expect that an increase of the Q-factor counteracts the tendency of effective damping at a given DOS in the spectrum around the driving frequency. In other words, there

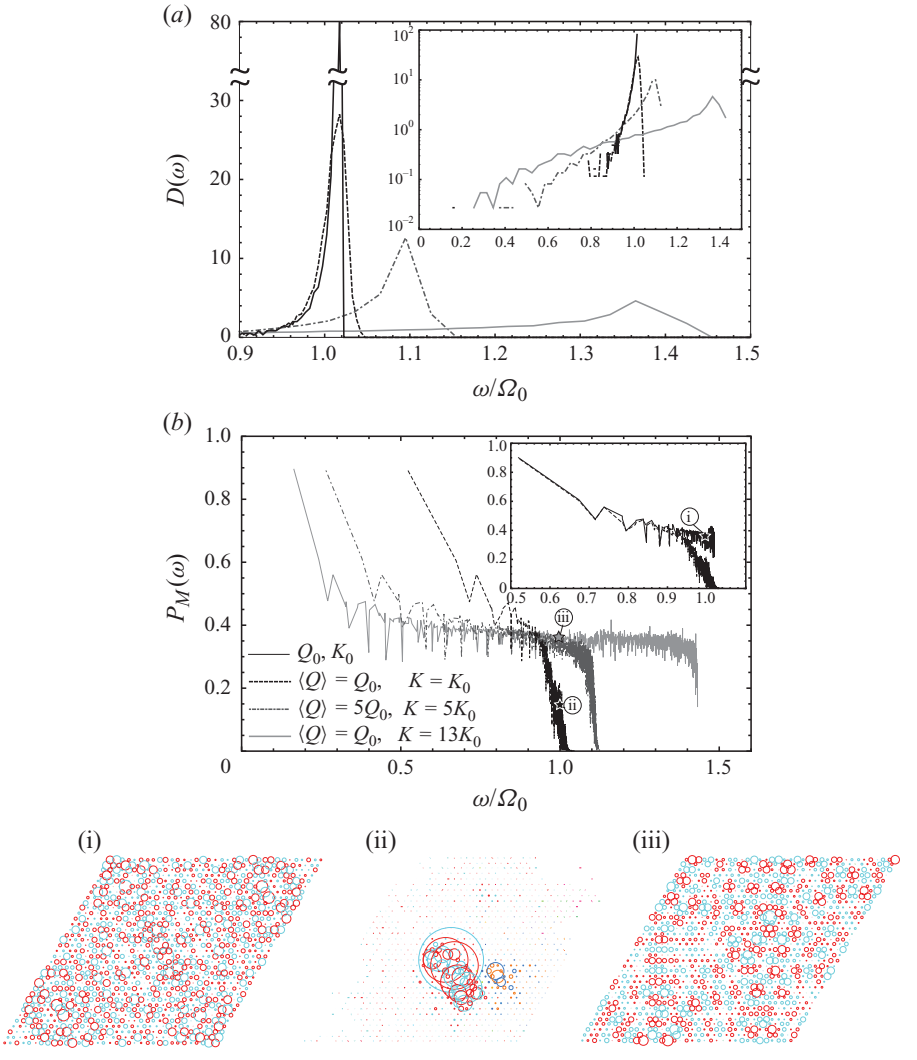

FIGURE 8. (Colour online) Spectrum, example modes and mode participation ratio for systems with disorder: (*a*) DOS for a system of $N = 1225$ bubbles. Initial bubble radii are coming from a Gaussian distribution with the width of 1 %. Different curves are for different values of the interaction parameter: the black-dashed curve is for parameters as in the monodisperse case (solid black line), but with 1 % of polydispersity; the grey dash-dotted one is for the case of average bubble radii being five times bigger (this also increases the sharpness of the resonances, which by itself has negligible influence on $D(\omega)$); the solid grey line is for the case in which the interaction parameter K is 13 times as strong. Note how the spectrum broadens once disorder is introduced. The inset shows the same data as in the main panel, but on a semi-log scale. (*b*) Mode participation ratio for systems as in (*a*). Even 1 % of polydispersity localizes modes at the high end of the spectrum. This effect is clearly seen in the inset of (*b*) where we plot P_M for the monodisperse (black solid line) and 1 % polydisperse (black-dashed line) clusters. To emphasize the effects of disorder, in (i) and (ii) we plot examples of modes that have approximately the same eigenfrequency, $\omega/\Omega_0 \approx 1$ (marked in figure 8(*b*)), but are either coming from the monodisperse (i) or 1 % polydisperse (ii) spectrum, respectively. Once K is increased (§ 2.2), localization gets suppressed, as captured with the solid grey line in (*b*). This can also be seen in the example mode (iii) (again for $\omega/\Omega_0 \approx 1$), that starts to recover plane-wave-like behaviour. In both (*a*) and (*b*), data points are connected by lines for clarity.

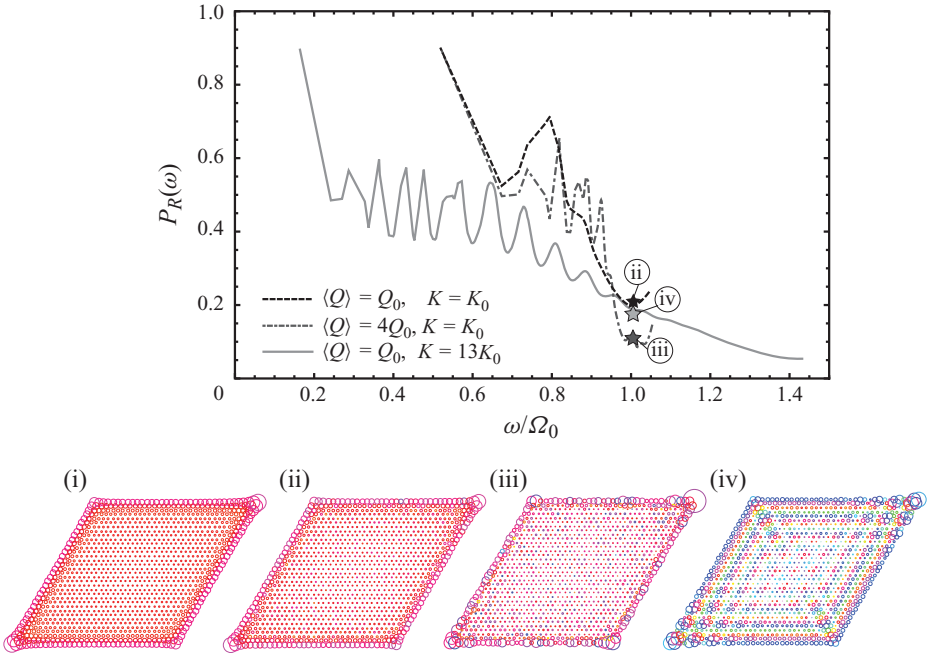

FIGURE 9. (Colour online) Main panel: response participation ratio as a function of driving frequency for a system of $N = 1225$ 1 % polydisperse bubbles. Subparts (i)–(iv) show response fields of different systems, driven with $\omega/\Omega_0 \approx 1$. For $\langle Q\rangle = Q_0$ and $K = K_0$ (see § 4), black-dashed line, $P_R(\omega)$ does not noticeably differ from the result of the monodisperse case. This can be seen when comparing (i) (response of the monodisperse system) and (ii) (response of the 1 % polydisperse system). Once we change $\langle Q\rangle$, through changing μ, and K, through changing d, oscillations in the plateau of $P_R(\omega)$ are introduced, which originate from $P_M(\omega)$ (figure 8(*b*)) and $P_M^{mono}(\omega)$ (figure 4) respectively. This can also be seen in (iii) and (iv) where a response of systems with $\langle Q\rangle = 4Q_0$, $K = K_0$ and $\langle Q\rangle = Q_0$, $K = 13K_0$ respectively is plotted. In the main panel, data points are connected with lines for clarity.

is a shift towards a single-mode response, as the weight is focused to fewer modes in the response (see § 2.5). We indeed see in figure 9(iii) that the edge-like response fields obtain local features, resembling the eigenmode shapes. On the other hand, the increase of K introduces a plane-wave-like modulation (figure 9(iv)), resembling the ideal system eigenmode shape. The increase of interactions between bubbles causes local out-of-phase oscillations and weakens the effect of disorder (phonon modes where nearby particles are oscillating in anti-phase are usually called 'optical modes' in condensed matter physics, Ashcroft & Mermin 1976).

5.1.2. *Mode and response participation ratio*

We also observe this change by analysing the behaviour of the mode and response participation ratios $P_M(\omega)$ and $P_R(\omega)$. In the mode participation ratio, $P_M(\omega)$, there are characteristic oscillations within the plateau (at $P_M(\omega) \approx 0.4$), which are not sensitive to the change of the Q-factor and K. The main panel of figure 8(*b*) demonstrates this robustness to changes in both the Q-factor and the interaction parameter through the mean initial bubble radius $\langle R_0\rangle$ (the curves have similar oscillation features, except for spanning different ranges in frequency). Looking at the response participation ratio $P_R(\omega)$ however reveals no oscillations when the Q-factor is kept at lower values,

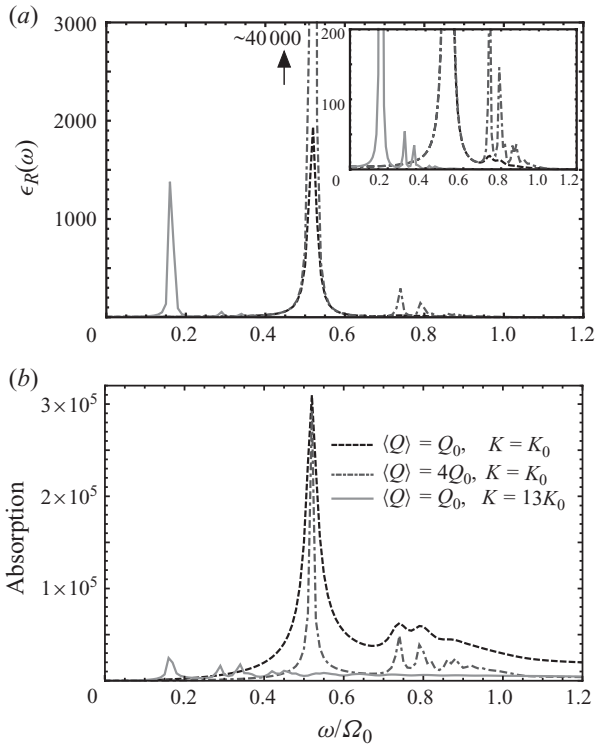

FIGURE 10. (*a*) Frequency response of the system of $N = 1225$, 1 % polydisperse bubbles to uniform driving. Contrary to previous plots, where data points at resonant frequencies are connected by straight lines, here the frequency is varying continuously. The pronounced peak in the case when $\langle Q\rangle = Q_0$ and $K = K_0$ (black-dashed line) is the response at the lowest-frequency mode. The inset shows a zoom-in of the main panel, where one can see a second, significantly smaller peak, corresponding to the response at the second lowest-frequency mode. Once we increase the $\langle Q\rangle$-factor (dot-dashed grey line), the existing peaks become more pronounced, and additional peaks appear (see the inset) as expected. Increasing the interaction parameter K stretches the spectrum and therefore moves the resonant peaks to lower frequencies, at the same time lowering their intensity. (*b*) Absorption, defined as the average dissipated energy in one period of oscillation under driving for systems as in (*a*).

figure 9 (black-dashed line). As the Q-factor is increased by changing μ (figure 9, grey dot-dashed line), the oscillations characteristic of the mode participation ratio $P_M(\omega)$ appear in the plateau of $P_R(\omega)$. This is a manifestation of the increasingly 'single-mode' nature of the response as the resonances are sharpened (i.e. Q-factor increased). There is an increased resemblance of the response and eigenmode shapes at a given (driving- and eigen-) frequency. On the other hand, the increase of the interaction parameter produces the same end result of oscillations of $P_R(\omega)$, but in a slightly different way: the response fields pick up the ideal system eigenmode shapes and consequently the oscillations from $P_M(\omega)$ as shown in figure 4.

5.1.3. *Frequency response and absorption*

We now address the implications of our results on experimentally observable quantities. We therefore study both the frequency response ϵ_R and the absorption of the system, when driven uniformly with some frequency ω, taken to be in the range 0 to $3\Omega_0$. In figure 10(*a*) we show the frequency response for three different sets

of values of Q and K. The pronounced peak in the case of $\langle Q \rangle = Q_0$ and $K = K_0$ (black-dashed line) is the response positioned at the lowest-frequency mode. This mode is the least damped one and follows the uniform driving the most, therefore giving the strongest response. The inset shows a zoom-in of the main panel, where one can see a second, significantly smaller peak, corresponding to the response at the second lowest-frequency mode. Once we increase the $\langle Q \rangle$-factor (dot-dashed grey line), the existing peaks become more pronounced, and additional peaks appear (see the inset) as is expected when the mode Lorentzians are narrower. As we have learnt from the DOS of the system with increased interaction parameter K (figure 8(*a*)), the spectrum becomes broader and stretches to lower frequencies, therefore shifting the response peak.

The absorption gives the time-averaged dissipated energy under driving. When driving is at a resonant frequency of a mode, that mode contributes to absorption proportionally to its damping coefficient and the overlap between the mode and the uniform driving vector (cf. § 3.3.2). In figure 10(*b*) we show the absorption curves for three different sets of values of Q and K as in (*a*). Although intuitively one expects high absorption for the modes with highest damping, which is the case for the highest-frequency modes of the system, we find the highest absorption around the lowest resonance, which is weakly damped but has the largest overlap with the uniform driving (black-dashed curve). The increase of the sharpness of the resonances lowers the damping and therefore the absorption (dot-dashed grey line).

5.2. *Strong disorder*

In this subsection we present results for the case of strongly disordered bubble clusters on a lattice, where we impose 20 % of polydispersity in initial bubble sizes. At this level of disorder, Anderson localization of modes is dominant and has a strong impact on the response to driving. The main effects of the strong disorder on the response, that we present in this subsection, are the appearance of *quasi-localized* low-frequency and high-frequency modes and *optical-like* delocalized high-frequency modes.

5.2.1. *Spectrum*

Demonstrative examples of eigenmodes in the presence of a strong disorder are shown in figure 11. In the lowest-frequency modes shown in figure 11(*a–c*) the underlying plane-wave-like pattern is still visible with an addition of a few strongly oscillating bubble groups, constituting a so-called quasi-localized mode. The rest of the spectrum is populated with very localized or quasi-localized modes, typical examples of which are shown in figure 11(*d–f*). The mode participation ratio, presented in figure 12(*b*), captures the localization behaviour well. Even the lowest modes show $P_M(\omega) \lesssim 0.4$, whereas most of the spectrum has $P_M(\omega) \sim 1/N$, i.e. is localized on the single-bubble level. The interaction parameter K induces the same qualitative change as in the low-disorder case, suppressing localization (less effectively in the high-end tail of $D(\omega)$).

As mentioned in the previous subsection, the DOS differs significantly from the monodisperse case, figure 12(*a*). The previously sharp single-bubble resonance peak (solid black line) becomes wide and somewhat shifts to lower frequencies (black-dashed line). A long tail appears in $D(\omega)$ up to $3\Omega_0$, sparsely populated by very localized modes – an example of a quasi-localized mode is depicted in figure 12(ii). The increase of the interaction between the bubbles and sharpness of the resonance parameters induce the same qualitative changes as in the low-disorder case. Localization and quasi-localization of the modes is captured by $P_M(\omega)$, figure 12(*b*).

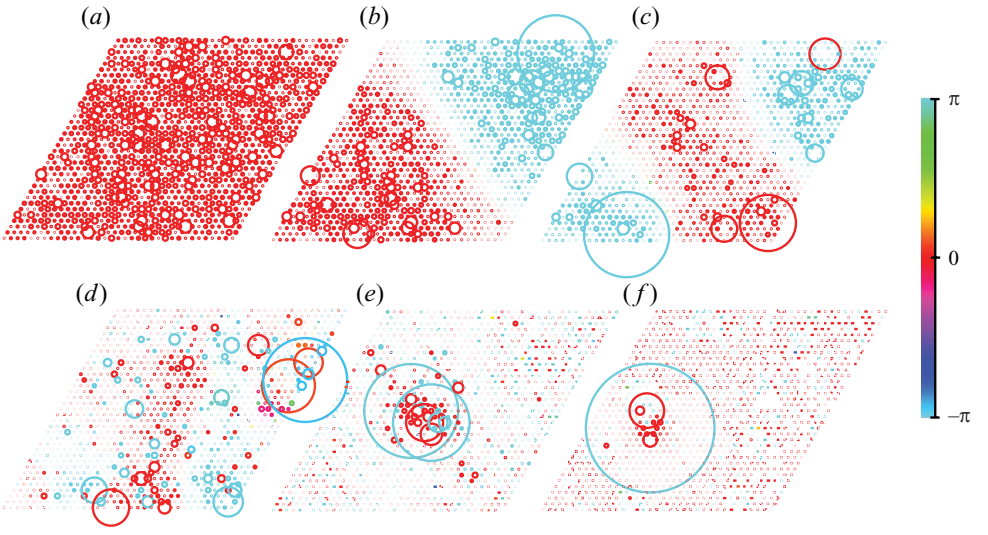

FIGURE 11. (Colour online) Six eigenmodes of the undriven, 20 % polydisperse 2D bubble cluster. For this illustration we chose (*a–f*) the 1st ($\omega/\Omega_0 \approx 0.47$), 2nd ($\omega/\Omega_0 \approx 0.58$), 5th ($\omega/\Omega_0 \approx 0.62$), 107th ($\omega/\Omega_0 \approx 0.76$), 607th ($\omega/\Omega_0 \approx 0.99$) and 1107th ($\omega/\Omega_0 \approx 1.39$) modes of the system with 1225 bubbles in rhombic geometry. The radii of the circles around the bubble location are proportional to the amplitude of the oscillation and the colour shows the phase. Note the strong Anderson-like localization of the eigenmodes.

Compared to the monodisperse case (solid black line and example mode depicted in figure 12(i)), 20 % of polydispersity localizes all the modes, the black-dashed line and example mode depicted in figure 12(ii). Once the interaction parameter is increased, like in the low-disorder case, modes start to recover the plane-wave-like character (figure 12(iii)).

5.2.2. *Response fields and response participation ratio*

In the response fields, figure 13, there is a recognizable underlying pattern similar to the low-disorder and monodisperse cases (plane-wave- and edge-like response, see figure 5), on top of which there are a large number of single-bubble oscillations with phases that spatially vary widely. This can be understood as an effect of the broadening of the DOS, which causes the mechanism of effective damping to be less efficient, figure 14. Instead of a washed-out response due to the contribution of many modes, the resulting fluctuating phase pattern that appears in these response fields is dominated by the underlying eigenmode, i.e. the mode at the driving frequency. A consequence of the observations above is that the response fields show localization. This is manifested in the calculated participation ratio, which is plotted in figure 15 (black-dashed curve). It is interesting to note that in the eigenmodes the disorder produces a large variation of amplitudes as well as phases at the single-bubble level, while in the response fields it is mostly the phase that significantly fluctuates.

A surprising feature is that the above explanations fail in the case of driving by the highest frequencies, where the response becomes *delocalized* (as in figures 13(*f*) and 15(ii)). We can however understand this by observing that the highest part of the spectrum $\Omega \lesssim \omega \lesssim 3\Omega$ is very sparse, containing just a few modes (see figure 12). This allows the lowest off-resonance mode having $\langle P|u_i\rangle \sim 1$ to dominate the contribution of the very few highest near-on-resonance eigenmodes, which have $\langle P|u_i\rangle \sim 0$. As we

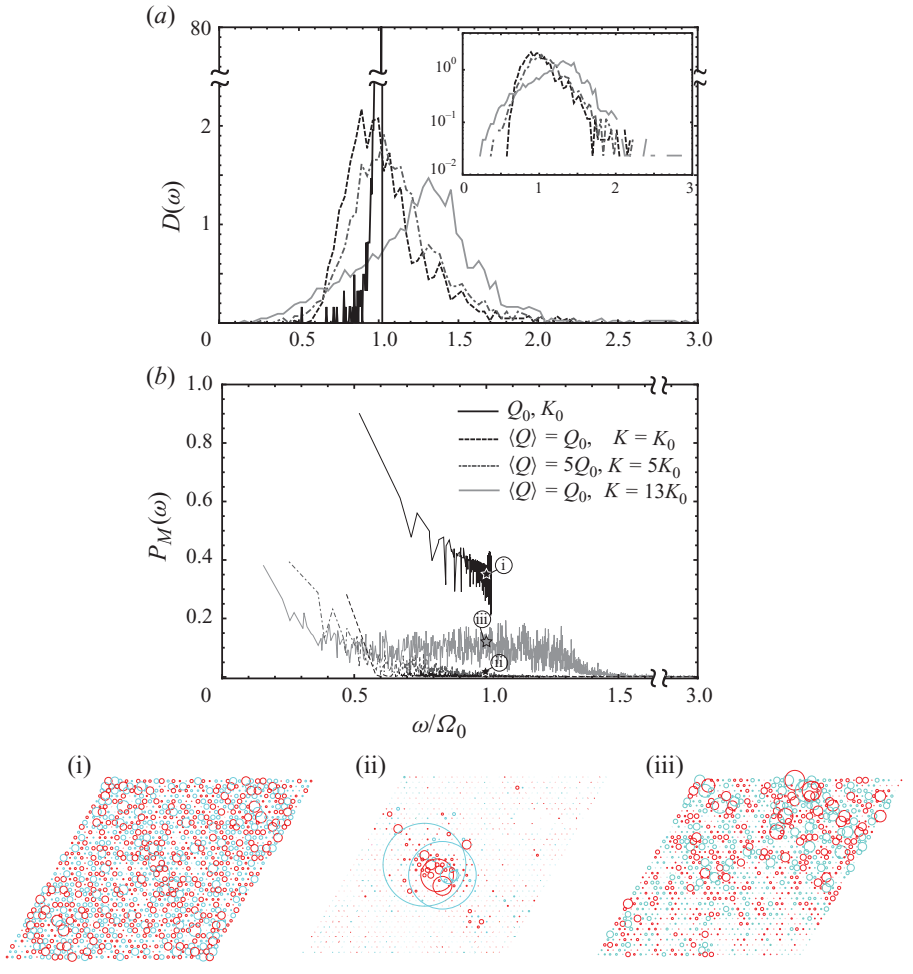

FIGURE 12. (Colour online) Spectrum, example modes and mode participation ratio for systems with disorder: (*a*) DOS for a system of $N = 1225$ bubbles. Initial bubble radii are coming from a Gaussian distribution with the width of 20 %. Different curves are for different values of the interaction parameter: the black-dashed curve is for parameters as in the monodisperse case but with 20 % of polydispersity; the grey dash-dotted one is for the case of average bubble radii being five times bigger (this also increases the sharpness of the resonances, which by itself has negligible influence on $D(\omega)$); the solid grey line is for the case of pitch decreased $\approx$13 times. For comparison, we also included $D(\omega)$ of the monodisperse system, solid black line. Note how the spectrum broadens with the increase of disorder. The inset shows the same data as in the main panel on a semi-log scale, with the monodisperse system omitted. (*b*) Mode participation ratio for systems as in (*a*). 20 % of polydispersity localizes basically all modes (black-dashed line) compared to the monodisperse case (solid black line). To emphasize the effects of disorder, in (i) and (ii) we plot examples of modes that have approximately the same eigenfrequency, $\omega/\Omega_0 \approx 1$, but are coming from the monodisperse and the 20 % polydisperse spectrum respectively. Once K is increased (§ 2.2), localization gets suppressed, as captured with the solid grey line in (*b*). This can also be seen in the example mode (iii) (again for $\omega/\Omega_0 \approx 1$), that starts to recover plane-wave-like quality. In both (*a*) and (*b*), data points are connected by lines for clarity.

increase the Q-factor, the highest-frequency modes become more localized, giving a more localized response. With increased interaction parameter, the response shifts towards the monodisperse response, with a pronounced edge-like structure.

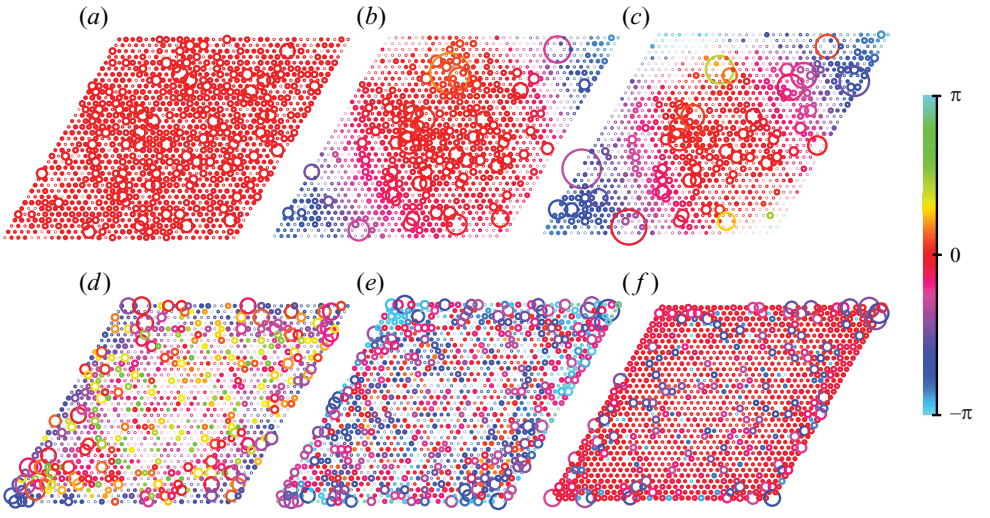

FIGURE 13. (Colour online) Response of the 20 % polydisperse 2D cluster of 1225 bubbles, when driven with (*a–f*) the 1st ($\omega/\Omega_0 \approx 0.47$), 3rd ($\omega/\Omega_0 \approx 0.60$), 5th ($\omega/\Omega_0 \approx 0.62$), 207th ($\omega/\Omega_0 \approx 0.82$), 507th ($\omega/\Omega_0 \approx 0.95$) and 1107th ($\omega/\Omega_0 \approx 1.39$) resonant frequencies. The radii of the circles around the bubble locations represent the amplitude of the oscillation and the colour shows the phase. Examples (*b*) and (*c*) are good representatives of the quasi-localized response fields, and (*f*) shows an example of a delocalized optical-like high-frequency response.

5.2.3. *Response excitability and mode contributions*

The basic influence of the sharpness of individual resonances and bubble–bubble interaction parameters is qualitatively the same as for the low disorder. In this case, increasing any of the two leads to localization of the highest driving frequency responses, albeit through different mechanisms, figure 15. With increasing sharpness, i.e. increase of the resonance factor for the highest modes, the contribution to response shifts away from the lowest mode, figure 14(*b*). The response becomes quasi-localized, resembling the highest eigenmode coupled to a uniform background. On the other hand, increasing K causes the system to behave more similarly to the ideal system (see also the discussion in § 5.1), and the response acquires the familiar edge shape along some local disorder events, again leading to localization, but of the edge type. The plot of response excitability, figure 14(*a*), shows that the highest driving response resembles the uniform driving field the most (black-dashed curve), but localizes at higher values of K or Q.

5.2.4. *Frequency response and absorption*

Figure 16 shows the frequency response and the absorption (§ 3.3.2) results for the strongly disordered systems. The essential features are interpreted in the same way as for the low-disorder case, § 5.1. The higher amount of polydispersity however explicates two main effects of disorder. Firstly, the low density of modes at lower frequencies is responsible for the appearance of more pronounced secondary peaks in the frequency response (figure 16(*a*)). Secondly, the relative intensity of the primary and secondary peaks changes considerably. At 1 % polydispersity, the ratio was around 100, while in the present case of 20 % polydispersity, it is lowered to around 60. This parameter is easily accessible to experiments and was considered in the analysis of micromeniscus oscillations (Rathgen *et al.* 2007), where the numerical

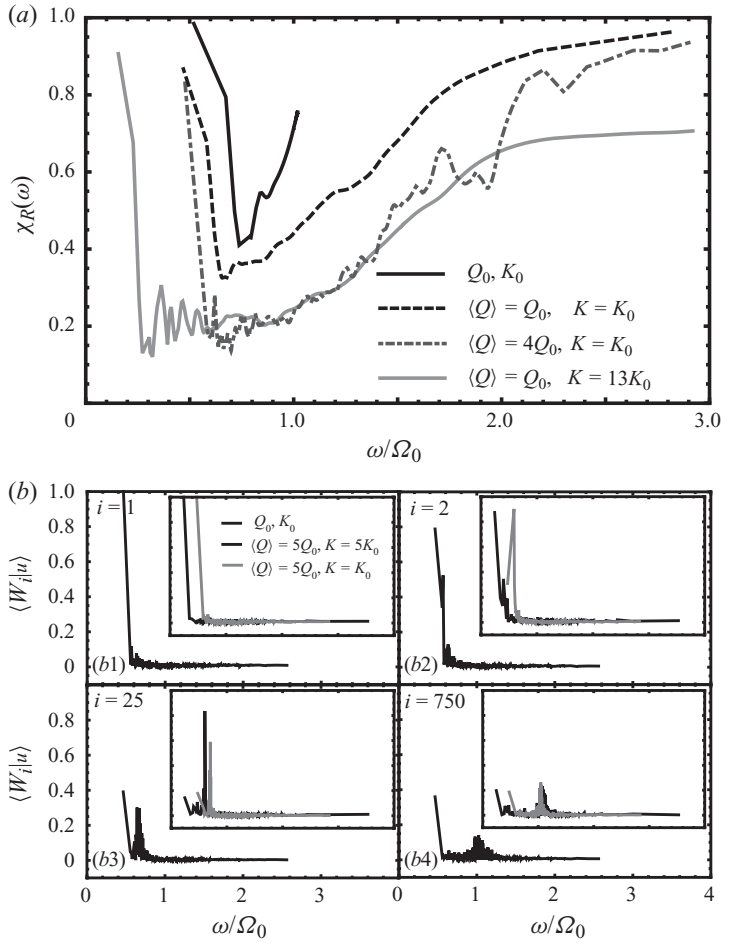

FIGURE 14. (*a*) Response excitability of a system of $N = 1225$, 20 % polydisperse bubbles. For most of the driving frequency range, $\chi_R(\omega)$ behaves as in the low-disorder case (black solid line). As we drive the system with highest eigenfrequencies, the response starts to look like the uniform driving field considerably. Increasing Q localizes the response; hence, the response resembles the driving field less. (*b*) Eigenmode contributions to the typical responses. Compared to the low-disorder case, the contribution of the lowest eigenmode is not significantly higher in every response. When a system is driven with a frequency within the now broad peak of $D(\omega)$, a number of modes $\ll N$ get excited (i.e. effective damping is less efficient), making the eigenmodes more visible in the response. The insets show the influence of the Q-factor and K parameters. In both (*a*) and (*b*), data points are connected with lines for clarity.

model predicted a much higher ratio than found in the measurement data. In that work, disorder is not explicitly taken into account, while our results suggest that it may be a decisive factor. The overall absorption becomes lower with the introduction of more disorder, figure 16(*b*).

5.3. *Exponential versus power-law localization*

Let us conclude this section with a more detailed analysis of the subtle issue of whether we observe true *exponential* Anderson localization or a *power-law*-like quasi-localization. Exponential localization is typical for systems with local

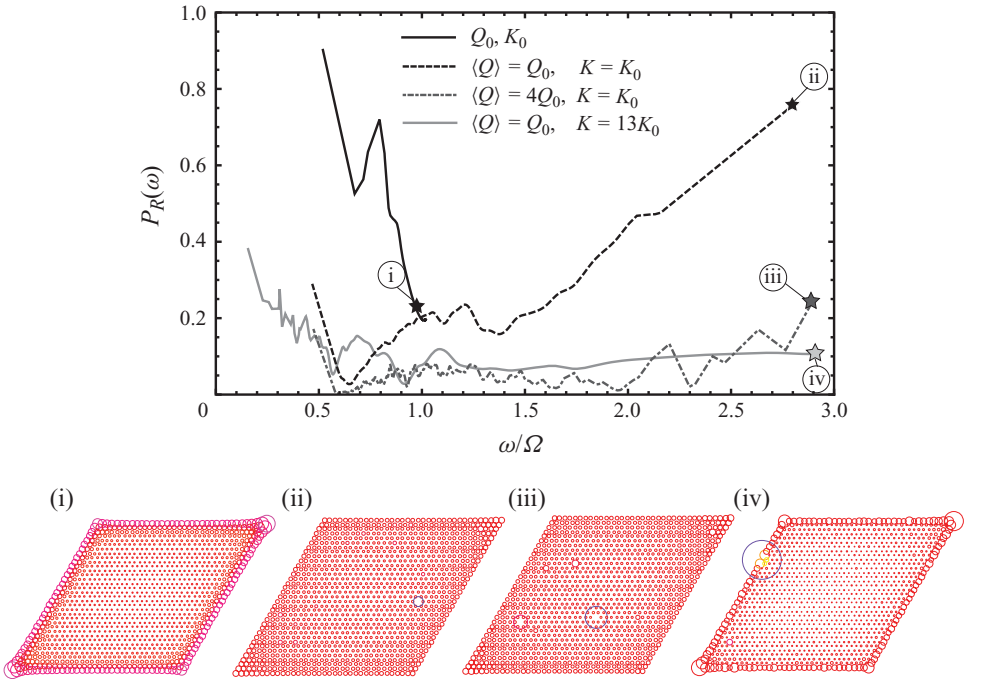

FIGURE 15. (Colour online) Response participation ratio of a system of $N = 1225$, 20 % polydisperse bubbles. Response to driving with frequencies within the peak of the now broad $D(\omega)$ is localized, while $P_R(\omega)$ increases for high-frequency driving (black-dashed curve), where the modes are sparse and effective damping suppressed (response to driving with the highest frequency is shown in (ii)). Once K and Q are increased (dash-dotted and solid grey line, respectively), the high-frequency response becomes localized, but in different ways, see the main text. The effect on the highest resonant frequency driving is shown in (iii) and (iv). The solid black curve shows the data for the monodisperse system as a comparison. In the plots, data points are connected by lines for clarity.

interactions, whereas for the bubble clusters analysed in this paper, the pressure-mediated interactions fall off inversely with distance, i.e. are long-ranged.

For illustrative purposes, we also simulated bubble clusters with the same parameters as in § 5.2 (i.e. 20 % polydispersity), but now artificially cutting off all long-range interactions, thus allowing only for the nearest-neighbour interactions. In order to see the quantitative effect of different interactions on the eigenmodes, we analyse the squared amplitude of each bubble, $|u_i|^2$, as a function of its radial distance from the maximal-amplitude bubble in the mode, for both short- and long-range interactions.

Figure 17 summarizes our findings. In (a) we plot the highest-frequency mode of a cluster with a long-range interaction and observe a power-law behaviour. For comparison, in the inset we plot both the mode from the main panel and the highest-frequency mode of a cluster with a short-range interaction. The difference between the exponential and the power-law localization is captured well. In (b), variables that we plot are the same as in (a), except that the mode which we study has an eigenfrequency close to the single-bubble resonant one.

As can be seen in the main panels of figure 17, the scaling exponent we observe varies from mode to mode and even within one mode due to the large scatter. Naïve analysis, that takes into account only the fact that the interaction potential between

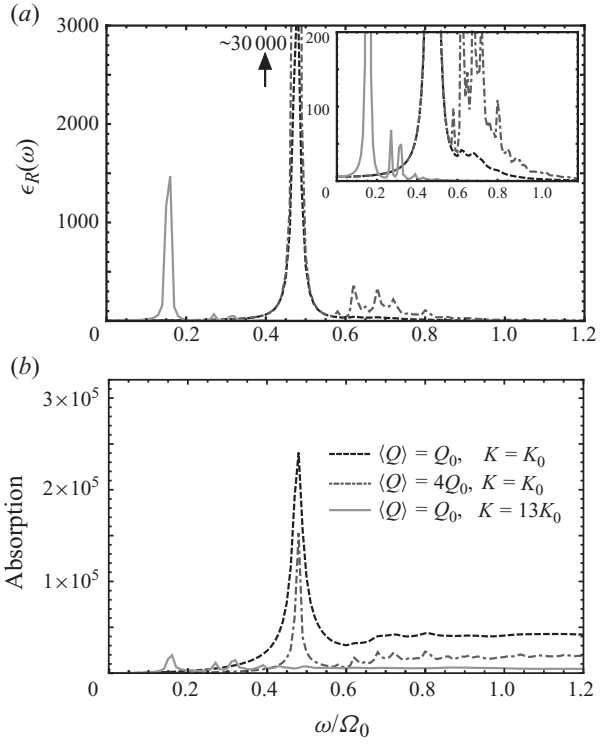

FIGURE 16. (*a*) Frequency response of the system of $N = 1225$, 20 % polydisperse bubbles to uniform driving. The pronounced peak in the case of $\langle Q\rangle = Q_0$ and $K = K_0$ (black-dashed line) is the response at the lowest-frequency mode. The inset shows a zoom-in of the main panel, where one can see a second, significantly smaller peak, corresponding to the response at the next few lowest-frequency modes. Note that the ratio of the primary and secondary peak heights is smaller here than at low disorder (figure 10). Once we increase the $\langle Q\rangle$-factor (dot-dashed grey line), the existing peaks become more pronounced, and additional peaks appear (see the inset) as expected (more peaks appear than at low disorder, the inset of figure 10(*a*), since here the modes are more sparse). Increasing the interaction parameter K stretches the spectrum and therefore moves the resonant peaks to lower frequencies, at the same time lowering their intensity. (*b*) Absorption, defined as the average dissipated energy in one period of oscillation under driving for systems as in (*a*).

bubbles is $\sim 1/r_{ij}$, would give $|u_i|^2 \sim 1/r^{-2}$. However, our modes rarely have only one bubble carrying the oscillation: most of the time we have groups of a few bubbles oscillating strongly, with differing phases. As an example, if maximal oscillation occurs for two bubbles which have opposite phases, a bubble far from them would essentially be subjected to a dipole interaction. If this would be the case, one should observe $|u_i|^2 \sim 1/r^{-4}$. We believe that our results reflect a combination of the two behaviours.

We finally mention that the amplitude decay of the response to uniform driving with different frequencies throughout the spectrum shows a power-law behaviour, with the power ≈ -0.75. The deviation from the intuitively expected power of -1 is ascribed to the presence of disorder, multiple large-oscillation centres, etc.

Next we attempt to reconcile our results on localization with the numerical and analytical findings of Sornette & Souillard (1988) and Ye & Alvarez (1998), who suggest Anderson localization of acoustic energy in bubble clouds and confirm its existence in a narrow frequency range around a single-bubble resonant frequency.

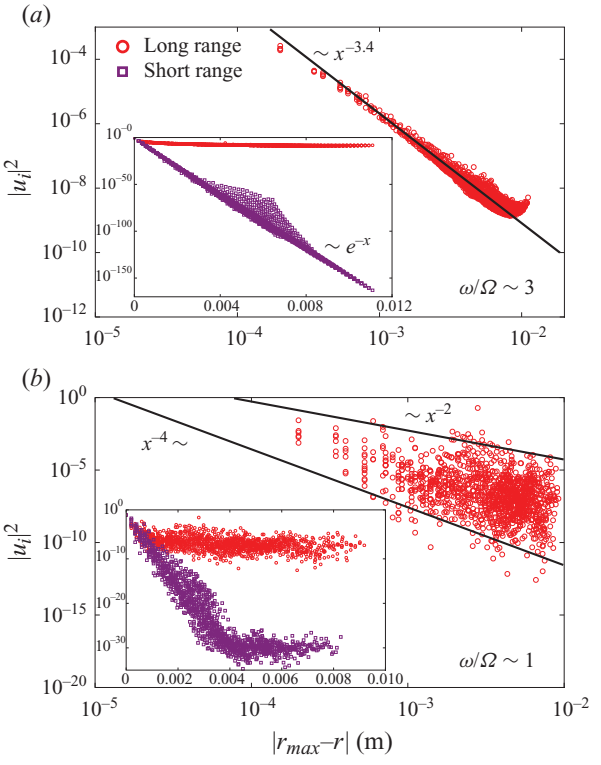

FIGURE 17. (Colour online) Quantitative comparison of the falloff of the amplitude $|u_i|^2$ of the eigenmodes as a function of distance r from the bubble with the largest oscillation amplitude, of a cluster with a long- and short-range interaction. Both clusters have $N = 2025$, 20 % polydisperse bubbles. (*a*) Log–log plot of the highest-frequency mode of a cluster with a long-range interaction. Power-law localization can be clearly seen. The inset compares the mode plotted in the main panel with the highest-frequency mode of a cluster with a short-range interaction. We use the log-linear scale to emphasize the exponential behaviour of the latter mode. (*b*) As in (*a*), but for the eigenfrequency close to the single-bubble resonant frequency.

These three-dimensional studies consider scattering of waves in a random medium, where randomness is controlled only by the distribution of bubbles (i.e. scatterers). The wave is driven at a point inside the medium and the interaction between the scatterers is of the form $e^{ikr_{ij}}/r_{ij}$. These studies consider the wave propagation from a local source, in contrast to the bubble dynamics due to a spatially uniform driving, that we analysed so far. Due to the change in sign of the $e^{ikr_{ij}}/r_{ij}$ interaction as the wave propagates through the medium, the long-range interaction becomes effectively short-range for finite k, with subsequently exponentially localized response.

To demonstrate that the oscillatory nature of the phase factor indeed changes the power-law localization into exponential localization as found by Sornette & Souillard (1988) and Ye & Alvarez (1998), we introduced the $e^{ikr_{ij}}/r_{ij}$ interaction into our framework and calculated the response to the driving of a single bubble with a frequency $\omega/\Omega_0 \sim 1$ for two values of the wave vector k: *(i)* for $k \sim \pi/d$, where the sign of the interaction alternates between every neighbour shell, and *(ii)* for $k \to 0$, where we recover the purely $1/r$ power-law interaction. The results of these calculations are plotted in figure 18 where the transition from the exponential localization for $k \sim \pi/d$ (panel (*a*)) to the power-law one for $k \to 0$ (panel (*b*)) is clearly visible.

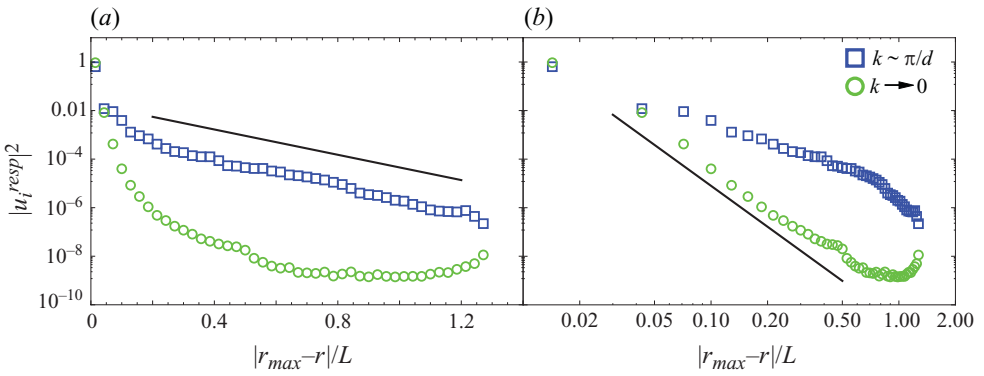

FIGURE 18. (Colour online) Quantitative comparison of the decay of the amplitude $|u_i^{resp}|^2$ of the response to driving of a single bubble with $\omega/\Omega_0 \sim 1$ as a function of distance r from the bubble with the largest oscillation amplitude, for $k \sim \pi/d$ and $k \to 0$. Both clusters have $N = 1225$, 1 % polydisperse bubbles (parameters are the same as for the clusters in figure 8 (black-dashed line)). (*a*) Log–lin plot of the two different responses. The solid straight line reveals the exponential localization of the $k \sim \pi/d$ limit. (*b*) Log–log plot of the two different responses, where the solid straight line signals the power-law localization of the $k \to 0$ limit.

5.4. *Polydisperse bubbles on a random underlying structure*

As noted in the introduction, the case of a random underlying structure is relevant for experimental 3D systems. In this section we consider bubbles drawn from a uniform distribution with 20 % polydispersity, located at random positions. In case the bubbles drawn had one or more neighbours closer than $3\langle R_0 \rangle$, they were not accepted in our random sample; this is simply in order not to have our representation of typical modes be dominated by bubble pairs which are very close and therefore strongly coupled. (In practical situations, the separation of the closest bubbles determines a maximum driving amplitude for nonlinear effects to take over or bubbles to merge.)

We find that all the conclusions and analysis of the results for this case are qualitatively the same as in the case of 20 % polydisperse bubbles on a lattice, considered in the preceding subsections. To avoid repetition, we omit the plots of the relevant quantities. Mode and response fields are shown in figures 19 and 20, and are analogous to figures 11 and 13.

The main quantitative difference, brought by the random underlying structure, is observed in figure 19(*b*,*c*). Namely, the quasi-localized character of the modes is more pronounced due to the fact that occasionally bubbles can be close to each other, taking the role of a single, relatively large bubble. The reason why the geometric disorder or also the dimensionality (2D versus 3D) plays only a minor role is that the effective interaction is long-ranged, so that each bubble interacts with many others. For the low frequency where nearby bubbles oscillate in phase, the geometric disorder then mostly affects the coupling of the bubbles, and hence the relative oscillation amplitude, but not the in-phase character. The details of the high-frequency modes, in which many bubbles oscillate in anti-phase, are more strongly affected, but as we have seen when driven by a particular frequency, the details of the modes effectively average out in the response due to the large density of such modes.

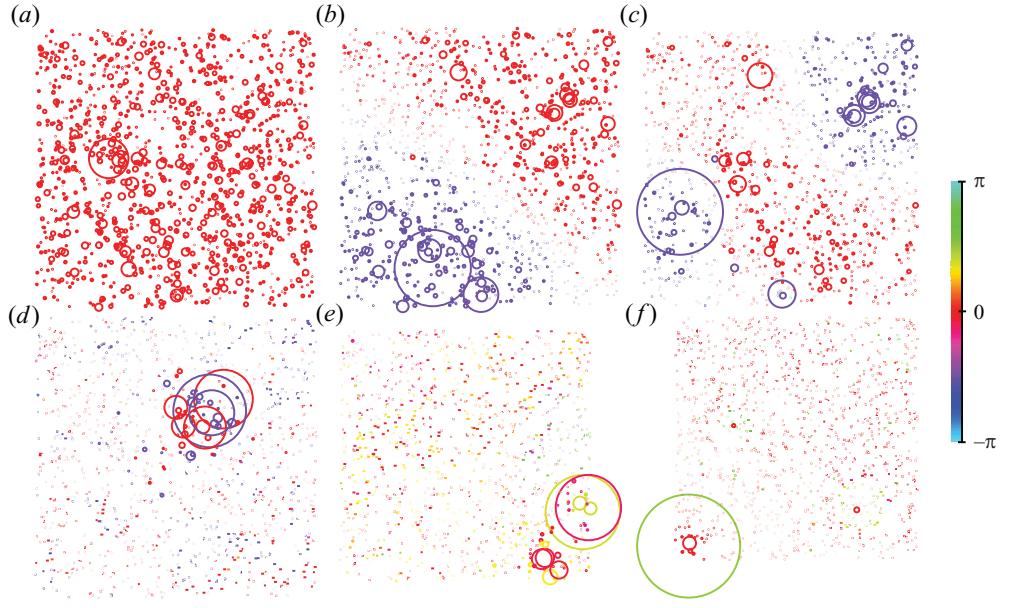

FIGURE 19. (Colour online) Six eigenmodes of the undriven, 20 % polydisperse 2D bubble cluster on a random underlying pattern. For this illustration we chose (*a–f*) the 1st ($\omega/\Omega_0 \approx 0.47$), 3rd ($\omega/\Omega_0 \approx 0.59$), 5th ($\omega/\Omega_0 \approx 0.61$), 107th ($\omega/\Omega_0 \approx 0.76$), 507th ($\omega/\Omega_0 \approx 0.95$) and 1107th ($\omega/\Omega_0 \approx 1.47$) modes of the system with 1225 bubbles in square geometry. The radii of the circles around the bubble locations are proportional to the amplitude of the oscillation and the colour indicates the phase. Note the strong Anderson-like localization of the eigenmodes.

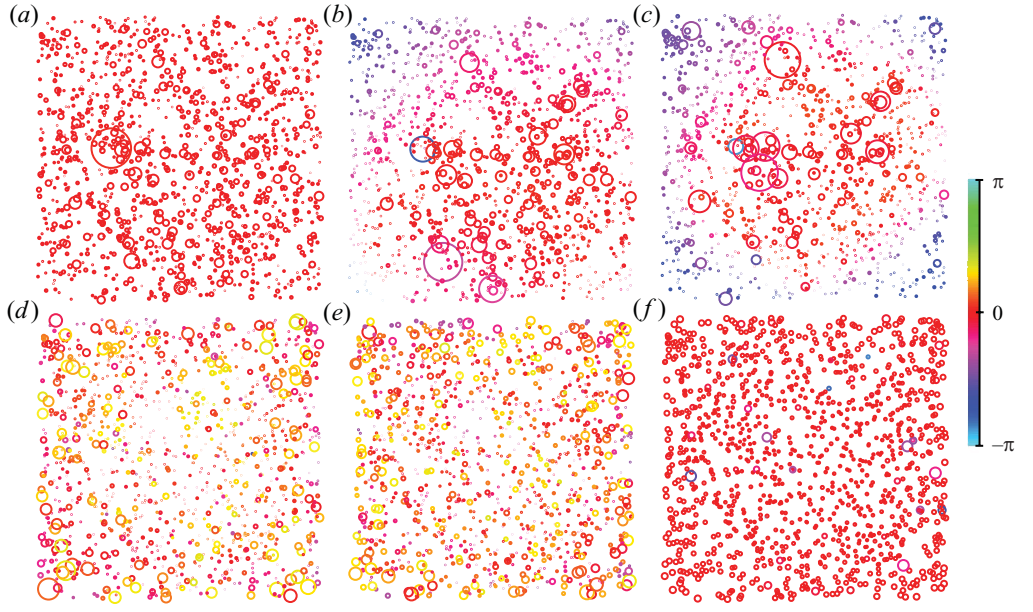

FIGURE 20. (Colour online) Response of the 20 % polydisperse 2D cluster of 1225 bubbles on a random underlying pattern, when driven with (*a–f*) the 1st, 3rd, 5th, 107th, 507th and 1107th resonant frequencies. The values of ω_d are the same as the resonant frequencies in figure 19. The radii of the circles around the bubble locations represent the amplitude of the oscillation and the colour the phase.

6. Outlook on experimental verification

To address which of our results could be tested directly in experiments, we come back to the experiments of Bremond *et al.* (2006*a*,*b*) and Rathgen *et al.* (2007) which had motivated the present study. In both of these studies, the collectively responding bubbles (or menisci) were fixed in space to a two-dimensional array. Such a geometrical constraint indeed eases the visualization of the bubble oscillations. The two most prominent collective features may be the existence of the pronounced edge states which first had been seen by Bremond *et al.* (2006*b*) and the pronounced low-frequency response as seen by Rathgen *et al.* (2007). We suggest to study how these collective features evolve with increasing bubble number N. Moreover, we suggest to study how more *localized* modes evolve once a disorder is introduced through a more polydisperse bubble size distribution. It would also be interesting to observe how the increase of viscosity affects the mode response and how the theoretical prediction – an enhanced multimode response – materializes in the experiments.

Though experimental observation may be easiest for 2D bubble configurations, an extension to the 3D case is possible: Garbin *et al.* (2007) succeeded to trap bubbles with optical tweezers, and exciting these bubbles with an acoustic field is clearly feasible. Presently however one is constrained to a few bubbles only, due to the technical complications.

Also the case of freely moving bubbles in 3D in an acoustical field is becoming experimentally accessible, thanks to the tremendous progress in 3D particle tracking velocimetry (Porta *et al.* 2001; Toschi & Bodenschatz 2009). Martinez-Mercado *et al.* (2010) have recently extended these methods to the tracking of thousands of bubbles. However, the obstacle that must be overcome is to provide sufficient spatial resolution to monitor the volume oscillation of each individual bubble. Due to the Bjerknes forces of first and second kind (Brennen 1995), the bubbles in an acoustic field organize in bubble streamers (Nyborg & Hughes 1967; Doinikov 2004; Pelekasis *et al.* 2004; Krefting *et al.* 2004), leading to a highly inhomogeneous bubble distribution in space.

For collectively oscillating bubbles in 3D the experimentally most accessible quantity may be the absorption spectrum, as shown in figures 10(*b*) and 16(*b*). Again, one can only expect to identify general features and trends with control parameters such as with the total number of bubbles or the viscosity.

In any case, bridging the gap between the present theoretical analysis of collectively (linearly) oscillating bubbles in either two or three dimensions and real-world experiments is still a major task ahead of us, but the present analysis of the important and sometimes surprising effects which arise in linear order is a good starting point for understanding the various phenomena discussed in the introduction.

This work is part of the research program of FOM, which is financially sponsored by NWO.

REFERENCES

Anderson, P. W. 1958 Absence of diffusion in certain random lattices. *Phys. Rev.* **109** (5), 1492–1505.

Arora, M., Junge, L. & Ohl, C. D. 2005 Cavitation cluster dynamics in shock-wave lithotripsy. Part 1. Free field. *Ultrasound Med. Biol.* **31** (6), 827–839.

Arora, M., Ohl, C. D. & Lohse, D. 2007 Effect of nuclei concentration on cavitation cluster dynamics. *J. Acoust. Soc. Am.* **121** (6), 3432–3436.

Ashcroft, N. W. & Mermin, D. N. 1976 *Solid State Physics*. Saunders College Publishing.

Bremond, N., Arora, M., Dammer, S. & Lohse, D. 2006*a* Interaction of cavitation bubbles on a wall. *Phys. Fluids* **18**, 121505.

Bremond, N., Arora, M., Ohl, C. D. & Lohse, D. 2005 Cavitation on surfaces. *J. Phys.: Condens. Matter* **17**, S3603–S3608.

Bremond, N., Arora, M., Ohl, C. D. & Lohse, D. 2006*b* Controlled multi-bubble surface cavitation. *Phys. Rev. Lett.* **96**, 224501.

Brennen, C. E. 1995 *Cavitation and Bubble Dynamics*. Oxford University Press.

Brennen, C. E. 2002 Fission of collapsing cavitation bubbles. *J. Fluid Mech.* **472**, 153–166.

Brenner, M. P., Hilgenfeldt, S. & Lohse, D. 2002 Single bubble sonoluminescence. *Rev. Mod. Phys.* **74**, 425–484.

Burns, P. N. 1996 Harmonic imaging with ultrasound contrast agents. *Clin. Radiol.* **51** (Suppl. 1), 50–55.

Busnaina, A. A., Kashkoush, I. I. & Gale, G. W. 1995 An experimental study of megasonic cleaning of silicon wafers. *J. Electrochem. Soc.* **142** (8), 2812–2817.

Calflisch, R. E., Miksis, M. J., Papanicolaou, C. & Ting, L. 1985 Effective equations for wave propagation in bubbly liquids. *J. Fluid Mech.* **153**, 259.

Colonius, T., Hagmeijer, R., Ando, K. & Brennen, C. E. 2008 Statistical equilibrium of bubble oscillations in dilute bubbly flow. *Phys. Fluids* **20**, 040902.

Crum, L. A. 1983 The polytropic exponent of gas contained within air bubbles pulsating in a liquid. *J. Acoust. Soc. Am.* **73**, 116–120.

d'Agostino, L. & Brennen, C. E. 1988 Acoustical absorption and scattering cross sections of spherical bubble clouds. *J. Acoust. Soc. Am.* **84** (6), 2126–2134.

d'Agostino, L. & Brennen, C. E. 1989 Linearized dynamics of spherical bubble clouds. *J. Fluid Mech.* **199**, 155–176.

Dayton, P. A., Chomas, J. E., Lum, A. F. H., Allen, J. S., Lindner, J. R., Simon, S. I. & Ferrara, K. W. 2000 Optical and acoustical dynamics of microbubble contrast agents inside neutrophils. *Biophys. J.* **80**, 1547–1556.

Doinikov, A. A. 2004 Mathematical model for collective bubble dynamics in strong ultrasound fields. *J. Acoust. Soc. Am.* **116**, 821.

Doinikov, A. A. & Zavtrak, T. 1996 On the 'bubble grapes' induced by a sound field. *J. Acoust. Soc. Am.* **99** (6), 3849–3850.

Garbin, V., Cojoc, D., Ferrari, E., Di Fabrizio, E., Overvelde, M. L. J., van der Meer, S. M., de Jong, N., Lohse, D. & Versluis, M. 2007 Changes in microbubble dynamics near a boundary revealed by combined optical micromanipulation and high-speed imaging. *Appl. Phys. Lett.* **90** (11) 114103-1–114103-3.

van Hecke, M. 2010 Jamming of soft particles: geometry, mechanics, scaling and isostaticity. *J. Phys.: Condens. Matter* **22**, 033101.

Hilgenfeldt, S., Brenner, M. P., Grossmann, S. & Lohse, D. 1998 Analysis of Rayleigh–Plesset dynamics for sonoluminescing bubbles. *J. Fluid Mech.* **365**, 171–204.

Hilgenfeldt, S., Lohse, D. & Brenner, M. P. 1996 Phase diagrams for sonoluminescing bubbles. *Phys. Fluids* **8** (11), 2808–2826.

Ida, M. 2004 Investigation of transition frequencies of two acoustically coupled bubbles using a direct numerical simulation technique. *J. Phys. Soc. Japan* **73**, 3026–3033.

Ida, M. 2005 Avoided crossings in three coupled oscillators as a model system of acoustic bubbles. *Phys. Rev.* E **72**, 036306.

Kamath, V., Prosperetti, A. & Egolfopoulos, F. N. 1993 A theoretical study of sonoluminescence. *J. Acoust. Soc. Am.* **94** (1), 248–260.

Krefting, D., Mettin, R. & Lauterborn, W. 2004 High-speed observation of acoustic cavitation erosion in multibubble systems. *Ultrason. Sonochem.* **11** (3–4), 119–123.

Kumar, S. & Brennen, C. E. 1993 Some nonlinear interactive effects in bubbly clouds. *J. Fluid Mech.* **253**, 565–591.

Landau, L. D. & Lifshitz, E. M. 1960 *Mechanics*. Pergamon.

Leighton, T. G. 1994 *The Acoustic Bubble*. Academic.

Leighton, T. G. 2004 From seas to surgeries, from babbling brooks to baby scans: the acoustics of gas bubbles in liquids. *Intl J. Mod. Phys.* B **18** (25), 3267–3314.

Liu, A. & Nagel, S. R. 2010 The jamming transition and the marginally jammed solid. *Annu. Rev. Condens. Matter Phys.* **1** 347–369.

Martinez-Mercado, J., Chehata-Gomez, D., van Gils, D., Sun, C. & Lohse, D. 2010 On bubble clustering and energy spectra in pseudo-turbulence. *J. Fluid Mech.* **649**, x.

van der Meer, S. M., Dollet, B., Voormolen, M. M., Chin, C. T., Bouakaz, A., de Jong, N., Versluis, M. & Lohse, D. 2007 Microbubble spectroscopy of ultrasound contrast agents. *J. Acoust. Soc. Am.* **121**, 648–656.

Mettin, R. 2005 *Bubble Structures in Acoustic Cavitation*. Research Signpost, Kerala, India.

Mettin, R., Akhatov, I., Parlitz, U., Ohl, C. D. & Lauterborn, W. 1997 Bjerknes forces between small cavitation bubbles in a strong acoustic field. *Phys. Rev.* E **56** (3), 2924–2931.

Mulvagh, S. L., DeMaria, A. N., Feinstein, S. B., Burns, P. N., Kaul, S., Miller, J. G., Monaghan, M., Porter, T. R., Shaw, L. J., Villanueva, F. S. & Am Soc Echocardiography Task Force 2000 Contrast echocardiography: current and future applications. *J. Am. Soc. Echocardiogr.* **13** (4), 331–342.

Noordzij, L. & van Wijngaarden, L. 1974 Relaxation effects, caused by relative motion on shock-waves in gas–bubble–liquid mixtures. *J. Fluid Mech.* **66** (OCT21), 115–143.

Nyborg, W. L. & Hughes, D. E. 1967 Bubble annihilation in cavitation streamers. *J. Acoust. Soc. Am.* **42** (4), 891.

Osborn, T., Farmer, D. M., Vagle, S., Thorpe, S. A. & Cure, M. 1992 Measurements of bubble plumes and turbulence from a submarine. *Atmos.-Ocean* **30** (3), 419–440.

Parlitz, U., Mettin, R., Luther, S., Akhatov, I., Voss, M. & Lauterborn, W. 1999 Spatio-temporal dynamics of acoustic cavitation bubble clouds. *Phil. Trans. R. Soc. Cond. Ser. A-Math. Phys. Eng. Sci.* A **357** (1751), 313–334.

Pelekasis, N. A., Gaki, A., Doinikov, A. A. & Tsamopoulos, J. A. 2004 Secondary Bjerknes forces between two bubbles and the phenomenon of acoustic streamers. *J. Fluid Mech.* **500**, 313–347.

Plesset, M. S. & Prosperetti, A. 1977 Bubble dynamics and cavitation. *Annu. Rev. Fluid Mech.* **9**, 145–185.

Porta, A. La, Voth, G. A., Crawford, A. M., Alexander, J. & Bodenschatz, E. 2001 Fluid particle accelerations in fully developed turbulence. *Nature* **409**, 1017–1019.

Prosperetti, A. 1977 Thermal effects and damping mechanisms in the forced radial oscillations of gas bubbles in liquid. *J. Acoust. Soc. Am* **61**, 17–27.

Prosperetti, A. & Lezzi, A. 1986 Bubble dynamics in a compressible liquid. I. First-order theory. *J. Fluid Mech.* **168**, 457–478.

Qin, S. P. & Ferrara, K. W. 2006 Acoustic response of compliable microvessels containing ultrasound contrast agents. *Phys. Med. Biol.* **51**, 5065–5088.

Rathgen, H., Sugiyama, K., Ohl, C. D., Lohse, D. & Mugele, F. 2007 Nanometer-resolved collective micromeniscus oscillations through optical diffraction. *Phys. Rev. Lett.* **99**, 214501.

Sangani, A. S. & Didwania, A. K. 1993 Dynamic simulations of flows of bubbly liquids at large Reynolds numbers. *J. Fluid Mech.* **250**, 307–337.

Sharpe, F. A. & Dill, L. M. 1997 The behavior of Pacific herring schools in response to artificial humpback whale bubbles. *Can. J. Zool.-Rev. Can. Zool.* **75** (5), 725–730.

Sheng, P. 1990 *Scattering and Localization of Classical Waves in Random Media*. World Scientific.

Sheng, P. 1995 *Introduction to Wave Scattering, Localization and Mesoscopic Phenomena*. Academic.

Smereka, P. 2002 A Vlasov equation for pressure wave propagation in bubbly fluids. *J. Fluid Mech.* **454**, 287–325.

Smereka, P. & Banerjee, S. 1988 The dynamics of periodically driven bubble clouds. *Phys. Fluids* **31**, 3519.

Sornette, D. & Legrend, O. 1992 Acoustic wave propagation in one-dimensional stratified gas–liquid media – the different regimes. *J. Acoust. Soc. Am.* **92** (1), 296–308.

Sornette, D. & Souillard, B. 1988 Strong localization of waves by internal resonances. *Europhys. Lett.* **7** (3), 269–274.

Toschi, F. & Bodenschatz, E. 2009 Lagrangian properties of particles in turbulence. *Annu. Rev. Fluid Mech.* **41**, 375–404.

Versluis, M., v. d. Heydt, A., Schmitz, B. & Lohse, D. 2000 How snapping shrimp snap: through cavitating bubbles. *Science* **289**, 2114–2117.

Vitelli, V., Xu, N., Wyart, M., Liu, A. J. & Nagel, S. R. 2010 Heat transport in model jammed solids. *Phys. Rev.* E **81**, 021301–021315.

Wang, Y. C. & Brennen, C. E. 1999 Numerical computation of shock waves in a spherical cloud of cavitation bubbles. *J. Fluids Eng. - Trans. ASME* **121** (4), 872–880.

van Wijngaarden, L. 1972 One-dimensional flow of liquids containing small gas bubbles. *Ann. Rev. Fluid Mech.* **4**, 369–396.

Wursig, B., Greene, C. R. & Jefferson, T. A. 2000 Development of an air bubble curtain to reduce underwater noise of percussive piling. *Mar. Environ. Res.* **49** (1), 79–93.

Xu, Ning, Vitelli, Vincenzo, Wyart, Matthieu, Liu, Andrea J. & Nagel, Sidney R. 2009 Energy Transport in Jammed Sphere Packings. *Phys. Rev. Lett.* **102** (3).

Ye, Z. & Alvarez, A. 1998 Acoustic localization in bubbly liquid media. *Phys. Rev. Lett.* **80** (16), 3503–3506.

Zeravcic, Z., van Saarloos, W. & Nelson, D. R. 2008 Localization of behavior of vibrational modes in granular packing. *EPL* **83**, 44001.

Zijlstra, A., Janssens, T., Wostyn, K., Versluis, M., Mertens, P. M. & Lohse, D. 2009 High speed imaging of 1 mhz driven microbubbles in contact with a rigid wall. *Solid State Phenomena* **145-146**, 7–10.